Proceedings of the XVII ECSMGE-2019
Geotechnical Engineering foundation of the future
ISBN 978-9935-9436-1-3

doi: 10.32075/17ECSMGE-2019-1108

XVII European Conference
ECSMGE 2019
Reykjavik
on Soil Mechanics
and Geotechnical Engineering

Hydraulic fills with special focus on liquefaction

Remblais hydrauliques en dédiant une attention particulière à la liquéfaction

A. Gens
Technical University of Catalonia (UPC), Barcelona, Spain

ABSTRACT: Hydraulic fills are often deposited in a loose state making them susceptible to liquefaction. The paper focuses on flow/static liquefaction, a phenomenon that has led to a number of catastrophic failures. The current understanding of flow/static liquefaction, based on the concepts of critical/steady state and state parameter, is reviewed. Theoretical concepts such as that of controllability lead to a more rigorous definition of the undrained instability phenomena associated with flow liquefaction. Hydraulic fills are often characterised by in situ tests. Advanced numerical analyses of the piezocone penetration test (CPTu) on soils exhibiting undrained softening are presented and discussed. Two case histories involving the liquefaction of hydraulic fills are described. The first one concerns a tailings dam where hydraulic fill liquefaction was a consequence of an independent foundation failure. Tailings liquefaction, however, was the major contributor to the devastating consequences of the failure. The second case is the failure of a harbour quay where backfill liquefaction was the immediate cause of the failure and its consequences. Some general considerations on the liquefaction of hydraulic fills close the paper.

RÉSUMÉ: Les remblais hydrauliques sont souvent déposés dans un état lâche, ce qui les rend vulnérables à la liquéfaction. L'article se concentre sur la liquéfaction statique, un phénomène qui a conduit à un certain nombre de ruptures catastrophiques. La compréhension actuelle de la liquéfaction statique, basée sur les concepts d'état critique ou stationnaire et de paramètre d'état, est examinée. Des concepts théoriques tels que celui de contrôlabilité conduisent à une définition plus rigoureuse des phénomènes d'instabilité non drainée associés à la liquéfaction statique. Les remblais hydrauliques sont souvent caractérisés par des essais in situ. Des analyses numériques avancées de l'essai de pénétration du piézocône (CPTu) sur des sols présentant un radoucissement non drainé sont présentées et discutées. Deux cas historiques impliquant la liquéfaction de remblais hydrauliques sont décrits. Le premier concerne une digue de résidus miniers où la liquéfaction du remblai hydraulique était la conséquence d'une rupture indépendante de la fondation. La liquéfaction des résidus a toutefois été le principal facteur des conséquences dévastatrices de cette rupture. Le deuxième cas se réfère à la faillite d'un quai de port où la liquéfaction du remblai était la cause immédiate de la rupture et de ses conséquences. Quelques considérations générales sur la liquéfaction des remblais hydrauliques sont exposées à la fin de l'article.

Keywords: Hydraulic fills; liquefaction; brittleness; tailing dams; quays

1 INTRODUCTION

Hydraulic fills are deposited in place by a flowing stream of water (Figure 1). They are used widely in different types of civil and mining engineering projects. Although the use of hydraulic fills in embankment dams has largely lapsed, posibly as a consequence of the Fort Peck dam failure (Davies et al. 2002), they are frequently used in land reclamation projects or in the construction of harbour quays and esplanades where dredged material is often available (van't Hoff and van der

Kolff 2012). Tailings from mining operations are also often deposited hydraulically in ponds although, as a result of some recent devastating failures, dry stacking is becoming more common. The particle size and grading of hydraulic fills can be very variable depending on the source material and the velocity of the deposition flow. Often, hydraulic fills exhibit significant particle-size segregation and a high degree of heterogeneity within the same area.

Figure 1. Deposition of a hydraulic fill

Hydraulic fills are often deposited in a loose state and are prone to liquefaction for a wide range of gradings from coarse sands to silts and any combination in between these limits. Although much liquefaction research has focused on sand, there is convincing evidence that presence of non-plastic fines may actually increase the potential for liquefaction (e.g. Lade and Yamamuro 1997).

Although, for a considerable period, there was a certain amount of confusion in liquefaction terminology, it is now generally accepted that it is useful to distinguish the phenomenon of flow/static liquefaction from that of cyclic liquefaction or cyclic mobility.

Flow/static liquefaction is associated with undrained softening behaviour and it often leads to catastrophic failures. Herein, the term flow liquefaction will be preferentially used because this type of liquefaction can also be triggered by cyclic loading. Carrera et al. (2011) have proposed the term 'true (or complete) liquefaction' for the extreme case when the deviator stress becomes zero at the end of undrained softening.

Cyclic liquefaction is not dependent on undrained softening and results from the accumulation of pore pressures during cyclic loading. Earthquake loading and storm loading on offshore structures are common examples of cyclic loading. The generation of pore pressures is enhanced if cyclic loading involves shear stress reversal. If, as a result of cyclic loading, very low effective stress states are reached, large deformations can occur although they largely stop once cyclic loading ends. The term cyclic mobility is usually applied to cases where zero effective stress is not approached and

only limited deformations are produced.

The typical undrained behaviour of non-plastic soils (including sands) is summarised in Figure 2 in a somewhat idealized manner. When the material is very loose, a frequent state in hydraulic fills, undrained softening occurs with a significant loss of strength after the peak is reached (A). The soil exhibits a compressive behaviour with a significant generation of pore pressures. In contrast, when the material is very dense, dilatant behaviour is obtained (C). An intermediate behaviour (B) is also observed sometimes where the final dilatant behaviour is preceded by a compressive phase with limited undrained softening. This intermediate behaviour will not generally lead to very large displacements and catastrophic failures. In this paper, only flow liquefaction is considered corresponding to the behaviour depicted as A in Figure 2. As discussed below, the terms loose or dense have proper meaning only in the context of a particular stress level.

Because flow liquefaction often results in catastrophic failures (Olson & Stark 2002, Jefferies & Been 2006, 2016), the phenomenon has been associated with many landmark cases involving hydraulic fills such as Fort Peck Dam (US) in 1938 (Casagrande, 1965), Lower San Fernando Dam (US) in 1971 (Seed et al. 1975,

Castro et al. 1989) and Nerlerk Berm (Canada) in 1982-1983 (Sladen et al. 1985b). Tailing dams have also provided many instances of flow liquefaction failures (Davies et al. 2002, Santamarina et al. 2019), e.g. the cases of Stava Fluorite Mine in 1985 (Chandler and Tosatti 1995), Sullivan Mine (Canada) in 1991 (Davies et al. 2002), Merriespruit Harmony Mine (South Africa) in 1994 (Fourie et al. 2001), Aznalcóllar tailings dam (Spain) in 1997 (Alonso and Gens 2006a) and Fundão Tailings Dam in 2015 (Morgenstern et al. 2016).

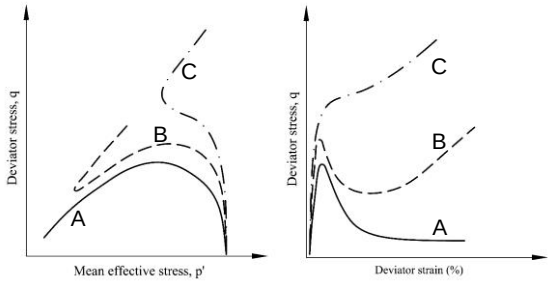

Figure 2. Typical modes of undrained behaviour

Naturally, flow liquefaction affects materials other than hydraulic fills. Important examples are Wachusett dam (US) in 1907 involving a sand fill placed (and lightly compacted) by carts (Olson et al. 2000), the failure of Aberfan spoil Tip No7 in Wales in 1966 involving uncompacted colliery waste (Bishop et al. 1969) and the dredged slopes of the guide bunds of the Jamuna bridge in Bangladesh (Yoshimine et al. 1999). The Aberfan case was significant not only due to the high number of casualties but also because it led to a significant advance in the understanding of flow liquefaction (Bishop et al. 1973). The Jamuna bridge case brought to the fore the unfavourable behaviour of micaceous sands compared to more conventional siliceous sands (Hight et al. 1999).

This paper focuses on flow liquefaction in hydraulic fills although many of the concepts used are also applicable to other soils undergoing undrained softening. Given the importance and frequent catastrophic consequences, a large amount of research has been performed on flow liquefaction. This contribution is by no means intended as a state-of-the-art of the topic, it simply presents and discusses some selected aspects that have been considered relevant. Because of space/time limitations, remedial and mitigation measures are not dealt with here.

The paper starts with an account of the current understanding of the mechanisms underlying the phenomenon of flow/static liquefaction, based on the concepts of critical/steady state and state parameter. It is shown that theoretical concepts such as that of controllability lead to a more rigorous definition of the undrained instability phenomena associated with flow liquefaction. The various forms of flow liquefaction triggering are presented next. Given that hydraulic fills are often characterised by in situ tests, some advanced numerical analyses of the piezocone test (CPTu) on soils exhibiting undrained softening are presented and discussed. Attention is given to the description of the constitutive law selected to represent undrained brittle behaviour. In order to provide context and relevance to the topic, two case histories involving the liquefaction of hydraulic fills are described: the failure of Aznalcóllar tailings dam and the failure of the Prat quay in Barcelona harbour. Some general considerations on the liquefaction of hydraulic fills close the paper.

2 MECHANISM OF FLOW LIQUEFACTION

2.1 Critical states and state parameter

The mechanism of flow liquefaction is now reasonably well understood although there are still some uncertainty and controversy regarding some of its specific aspects. Here, only a summary description is given. Flow liquefaction mechanism is best examined in the context of the notion of critical state. The concept was introduced by Casagrande (1936) who observed that, in shear box tests, loose sands contracted

and dense stands dilated until reaching approximately the same void ratio after large displacements (Figure 3). This final void ratio was called the critical void ratio. No further volume change was observed once the sand had reached this final state. Critical void ratio turned out to be stress dependent (Taylor 1948).

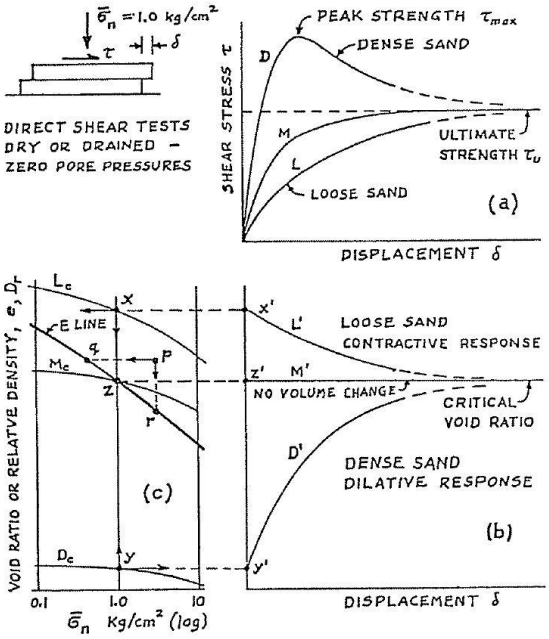

Figure 3. Critical void ratio from direct shear tests (Casagrande 1975)

More generally, the condition of a soil undergoing shear strains under constant stress and with no volume change is called the critical state of the soil and it is a key element of the critical state frameworks and models (Schofield and Wroth 1968). The relationship between critical void ratio and effective stress (usually the mean effective stress is selected) is the critical state line or critical state locus, CSL (Figure 4). Sometimes the line is alternatively called the steady state line (SSL) although the definitions of steady state and critical state are slightly different, as discussed below. Although, the critical state locus is often approximated as a straight line in semi-log space, in fact the line is often bilinear or curved (e.g. Figure 5). The increase of the slope of the CSL at high stresses is often attributed to particle crushing although it is debatable whether, in the case of evolving materials, a single plane is more appropriate than a single line (Muir Wood 2007, Ciantia et al. 2019). It is interesting to note that early applications of critical state or critical void ratio concepts were made in the investigation of the flow liquefaction of Fort Peck dam; flow liquefaction and critical states appear to have been associated from the start.

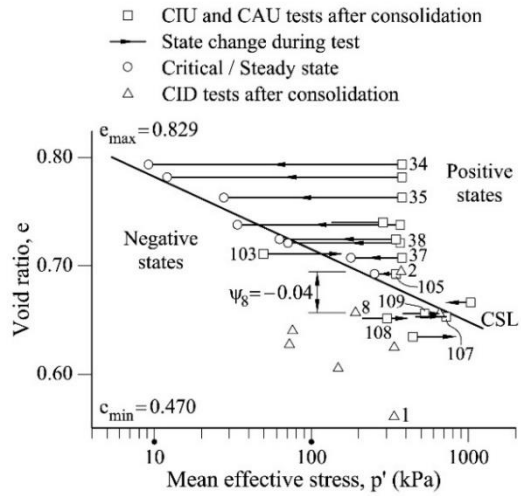

Figure 4. Critical state line for Kogyuk 350/2 sand (modified from Been and Jefferies 1985)

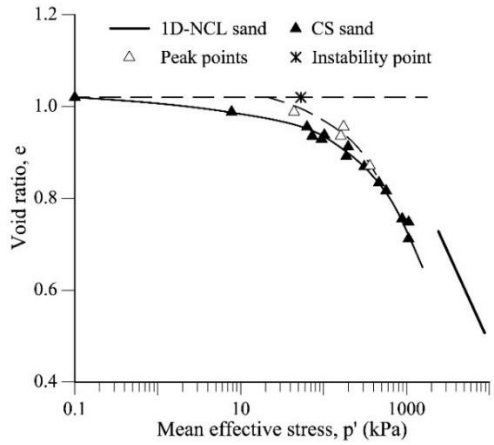

Figure 5. Critical state line for Stava tailings (modified from Carrera et al. 2011)

An important contribution to the characterisation of the behaviour of soils has been the concept of state parameter, ψ. It was anticipated in Wroth and Basett (1965) but it has been incorporated into the mainstream of soil mechanics though the work of Been, Jefferies and co-workers. In their seminal paper (Been and Jefferies 1985), the state parameter is simply defined as the difference between the current void ratio and the void ratio at critical state for the same mean effective stress (Figure 6). In this way, the character of a soil, loose or dense, is automatically related to the magnitude of the effective stress. An advantage of referring the state of the soil to its critical state is that the natural alternative, the normal consolidation line, is difficult to identify in some materials (especially granular ones) and it may be strongly dependent on the initial conditions of the specimen. Been and Jefferies (1985) showed that the state parameter provided a more unified perspective of soil behaviour, especially for sands. Naturally, the behaviour of the soils cannot depend uniquely on the state parameter; other parameters such as fabric and anisotropy are required (Been et al. 1991). It is again interesting to note that the development of the state parameter concept was made in the context of providing a rational engineering approach to the construction of structures using undensified hydraulic sand fills.

2.2 Undrained softening

The mechanism underlying flow liquefaction is illustrated by the undrained stress path and stress-strain curve of Figure 7; it corresponds to behaviour type A of Figure 2. The key feature is that the deviatoric stress reaches a peak (sometimes called instability point) and the material softens afterwards, i.e. the undrained shear strength reduces. The stress path and stress-strain curve finally reach a point where no further pore pressure develops and deviatoric strains increase indefinetely, i.e. the critical state (CS) has been reached. Accordingly, the end point will be basically controlled by void ratio and effective stress magnitude following the CSL relationship. Large positive pore pressures develop corresponding to the compressive nature of the soil; hence development of flow liquefaction is closely related to positive values (or even slightly negative) of the state parameter. If the void ratio is very high and plots above the critical state value at very low mean effective stress (see Figure 5), then the stress path will go all the way down to zero deviator stress (Carrera et al. 2011, Yamamuro and Lade 1998). As indicated above, this case has been named 'true liquefaction' on the basis that the shear strength of the soil now truly becomes zero (Carrera et al. 2011). However, as undrained softening (without reaching zero strength) can also lead to flow liquefaction and, consequently, to catastrophic outcomes, no distinction will be made in this paper between undrained softening and true liquefaction although, naturally, the consequences of a failure would be more drastic if a soil does reach a zero shear strength value.

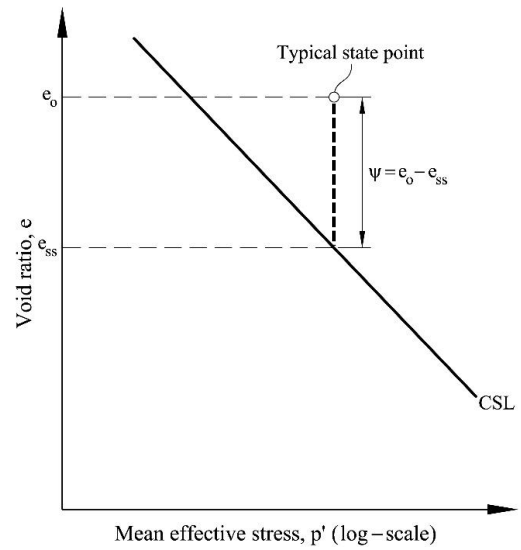

Figure 6. Definition of state parameter, ψ (modified from Been et al. 1991)

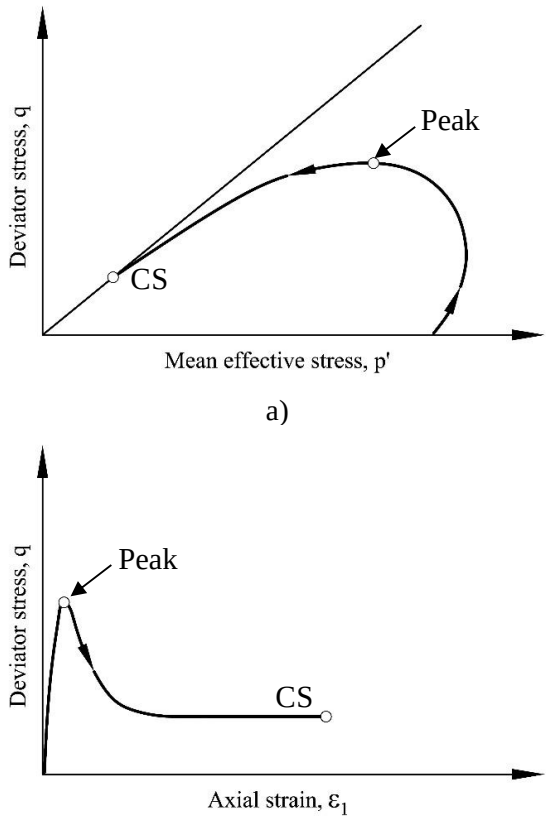

Figure 7. Undrained softening: a) effective stress path; b) stress-strain curve

The association of flow liquefaction with undrained softening and pore pressure increase was already clearly identified in the stress-controlled tests carried out by Castro (1969) (Figure 8). It should be noted that, because of the stress-controlled nature of the tests, the strain rate after peak is several orders of magnitude larger than the strain rate before the peak, raising some questions about potential rate effects. The same undrained softening mechanism was also recognized by Bishop et al. (1969) and Bishop (1973) as the ultimate cause underlying the Aberfan disaster. To quantify the magnitude of softening, Bishop (1973) proposed the definition of a brittleness index that, for an undrained case, reads:

$$I_B = \frac{(c_u)_f - (c_u)_r}{(c_u)_f} \quad (1)$$

where $(c_u)_f$ is the peak undrained shear strength and $(c_u)_r$ is the residual (critical state) undrained shear strength. The peak point and the critical state have in fact very different characteristics as discussed in the next two subsections.

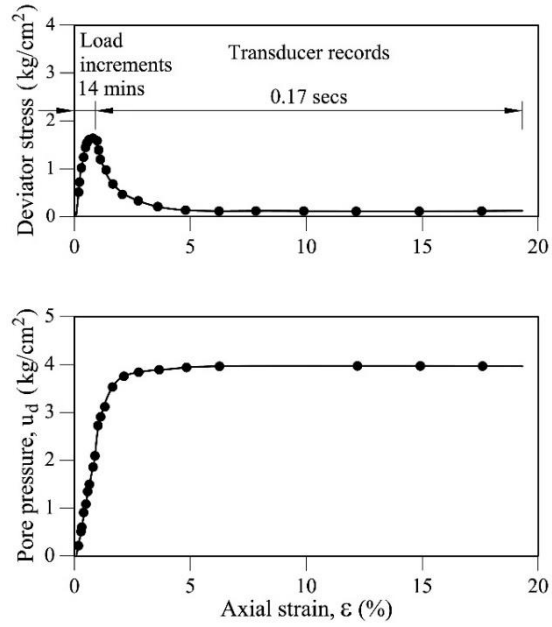

Figure 8. Results of a stress controlled test on loose Banding sand (modified from Bishop 1973, data from Castro 1969): deviator stress-axial strain curve and pore pressure-axial strain curve

2.3 Critical/steady state

As indicated above, the final state of the soil after undrained softening corresponds closely to the definition of critical state (Jefferies and Been 2006). In terms of effective stress, the mobilised friction angle corresponds to that of critical state (or constant volume). In the context of flow liquefaction, the final state has also been called steady state. It has been defined by Poulos (1981) as follows: 'the steady state of deformation of any mass of particles is that state in which the mass is

continuously deforming at constant volume, constant normal effective stress, constant shear stress and constant velocity'. Thus, the main difference compared to critical state is that a constant velocity is additionally prescribed. The notion of steady state has been central to the development and application of the steady state approach to liquefaction evaluation (Poulos et al. 1985). Often, however, critical state and steady state are used interchangeably. The final strength after softening has also been called liquefied strength or residual strength.

Been et al. (1991) found the same critical state for Erksak sand independently of strain rate even when comparing strain-controlled and stress-controlled tests. However, they acknowledge that different results may be obtained testing other materials such as finer silty sands. In fact, the issue of the uniqueness or otherwise of the critical state line has a long history. Casagrande (1975) and Alarcon et al. (1988) distinguished between "S" and "F" lines. The "S" line would correspond to drained triaxial tests whereas the "F" line would correspond to undrained triaxial tests. In fact, this distinction cannot be considered correct within the framework of the effective stress principle, as drained/undrained situations are boundary conditions that should not affect the fundamental behaviour of the soil.

However, at observational level, the question of uniqueness of the critical state line remains largely unresolved. Some studies have found a unique critical state line (e.g. Been et al 1991, Ishihara 1993, Fourie and Papageorgiou 2001, Carrera et al. 2011, Li et al. 2018) whereas non uniqueness has been reported from other sources (Konrad 1993, Kuerbis and Vaid 1988, Vaid et al. 1990, Hird and Hassona 1990). Coop (2015) has identified a range of soils (named 'transitional soils') where the critical state framework faces significant limitations.

In any case, account should be taken of the experimental difficulties of determining the critical state accurately. They arise from different causes: the limitation of the axial strain that can be achieved in the triaxial apparatus, the need for area and membrane penetration corrections, accounting for volume changes during backpressure saturation, the effects of strain localisation, and incorporating inertial effects in the interpretation of stress-controlled tests. Probably, more research is required on this topic especially at the very high strain rates involved in field liquefaction phenomena.

2.4 Peak strength

Whereas the final state after undrained softening is reasonably well established based on critical state considerations, there are less conceptual constraints concerning the point of maximum (peak) strength that signals the onset of instability. It can be noted that peak strength is reached with a mobilised friction angle well below the critical state one. Because peak strength values increase in an approximately linear manner with mean effective stress, it is tempting to join the different peak state points to establish a kind of failure criteria in terms of effective stresses. Two different proposals have been made (Figure 9): a collapse line that passes through the steady state point (Sladen et al. 1985a, Ishihara 1993) and a flow liquefaction line that passes through the origin (Vaid and Chern 1985, Lade 1993). Yang (2002) puts forward a proposal, based on the state parameter, to reconcile the two concepts. Probably, the different existing approaches just reflect the variability and lack of conceptual restrictions for this soil state. It has been observed, for instance, that peak strength is dependent on strain rate and consolidation stress path (Gens 1982). From both a fundamental and practical viewpoint, peak conditions are better considered based on undrained shear strength considerations rather than on effective stress parameters.

An important factor that has not been sufficiently attended to, concerns the effect of anisotropic consolidation. For instance, the tests performed by Castro (1969) show a clear dependence of undrained sand behaviour on the nature of the initial stress state (Figure 10).

However, much of the laboratory experimental work on flow liquefaction has been performed on isotropically consolidated samples. Obviously, this condition does not correspond to the in situ stress state of a hydraulic fill where normally consolidated Ko conditions (and therefore anisotropic stresses) should prevail.

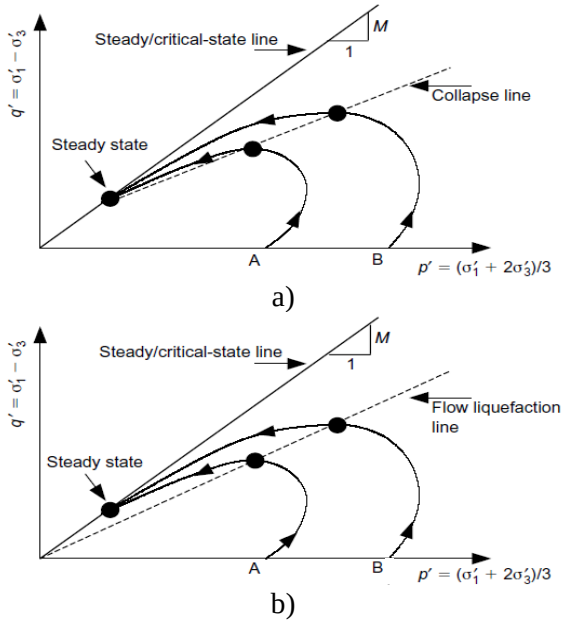

Figure 9. Schematic diagram for peak strength envelopes (Yang 2002): a) collapse line concept; b) flow liquefaction line

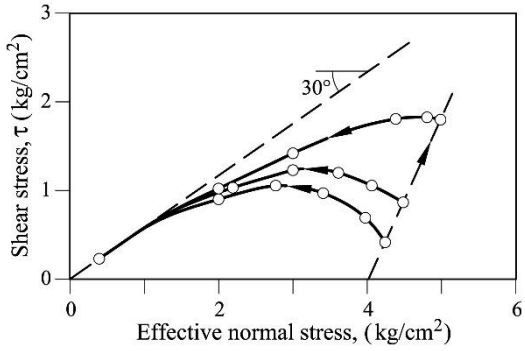

Figure 10. Stress paths for anisotropically consolidated undrained tests on saturated Banding sand (modified from Bishop 1973, data from Castro 1969)

Strong evidence of the effect of the initial state is provided by Fourie and Tshabalala (2005). They performed undrained triaxial tests on specimens of Merriespruit gold tailings and examined the results for each value of fines content. As an example, Figure 11 shows the results from samples with 20% fines consolidated isotropically and anisotropically. The differences are apparent especially concerning the peak strength and the possible flow liquefaction line. Thus the stress ratio (η=q/p') at which peak is reached is about 0.6 for the isotropically consolidated samples but it rises to 0.9 for the anisotropically consolidated ones. A proper consideration of peak strength and associated undrained softening behaviour should be based on tests that adopt the correct initial stress state. Indeed, a general perspective should ideally also include the effect of principal stress orientation and intermediate principal stress (Symes et al. 1984).

2.5 Instability conditions

Much work has been done to deal with material instability from a rigorous theoretical mechanics perspective (e.g. Nova 1989, 1994, Darve 1994, Borja, 2006, Nicot et al. 2007, Andrade 2009). It is interesting to examine, from this general point of view, the instability event that takes place when the deviator stress reaches the value of peak strength. At that point (point P in Figure 12), there is an apparent inconsistency. When an undrained test reaches its peak strength, the material softens and collapses, especially under stress-controlled conditions. However, if the test is performed drained, the material crosses point P without any visible instability.

This paradox is usefully explored using the important concept of controllability developed by Nova and co-workers (Nova 1994, Imposimato and Nova 1998). The concept addresses the role of control conditions in the onset of failure. The response of a material can be expressed as (Buscarnera and Whittle 2013):

$$\Phi = \mathbf{X}\Psi \tag{2}$$

where Φ is the combination of control stresses and strains whereas Ψ is the combination of stresses and strains that define the material response. $\mathbf{X}$ expresses the relationship between the applied variables and the material response. Stresses and strains in Φ and Ψ must be work-conjugate. Loss of controllability arises when:

$$\det \mathbf{X} = 0 \tag{3}$$

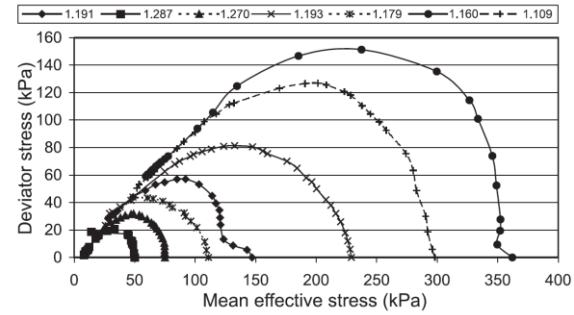

a)

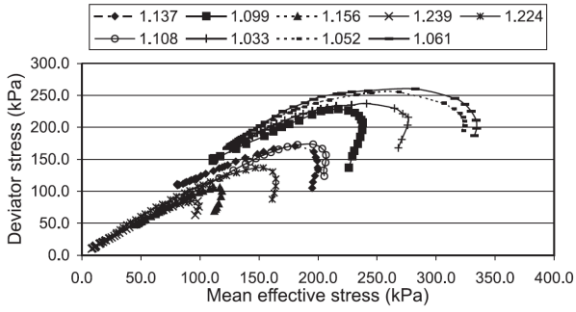

b)

Figure 11. Stress paths from undrained triaxial compression tests on Merriespruit gold tailings with 20% fines (Fourie and Tshabalala 2005):
a) isotropically consolidated specimens;
b) anisotropically consolidated specimens

The basic difference between a drained and undrained test lies in their different control variables. Specifically, in an undrained test a negligible volume change conditions is prescribed. Under those conditions, it is possible to define, within an elastoplastic framework, a critical liquefaction modulus as:

$$H_{LIQ} = -\frac{\partial f}{\partial p'} K \frac{\partial g}{\partial p'} \tag{4}$$

where f is the current yield surface, g the plastic modulus and K the elastic volumetric modulus.

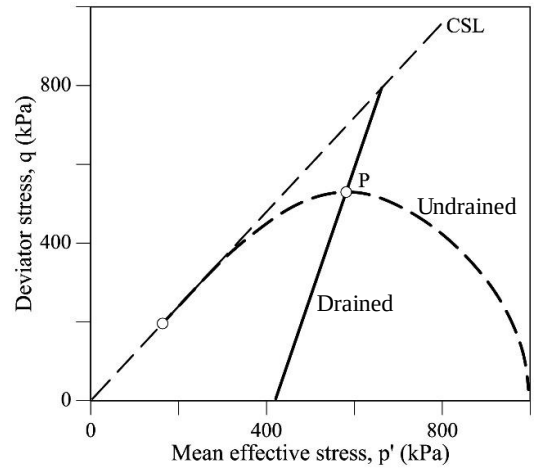

a)

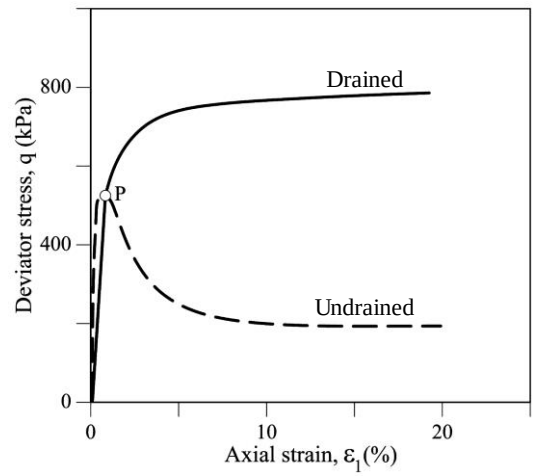

b)

Figure 12. Drained and undrained behaviour of a soil exhibiting undrained softening: a) effective stress paths; b) stress-strain curves

Controllability is lost when the difference between hardening modulus and the critical liquefaction modulus (Λ)

$$\Lambda_{LIQ} = H - H_{LIQ} \tag{5}$$

becomes zero or negative.

This situation corresponds to the onset of liquefaction and Λ has been called stability index because it constitutes a scalar measure of stability (Buscarnera and Whittle 2013). In fact, Buscarnera et al. (2011) have shown that that it is possible to consider together controllability, uniqueness and existence of the incremental response of the material depending on the sign of the stability index.

Instability can now be re-examined with reference to Figure 13 that shows the simulation of an undrained triaxial test on a loose sample of Toyoura sand using the elastoplastic model MIT-S1 (Pestana and Whittle 1999). Figure 13a presents the stress-strain curve together with the evolution of the stability index. It can be noted that the stability index becomes zero when the material reaches the peak undrained strength and it has a negative value during the softening branch of the test. The index goes back to zero on reaching critical state. The two components of the stability index, plastic modulus and critical liquefaction modulus, are plotted separately in Figure 13b. It is interesting to note that the plastic modulus is positive (i.e. strain hardening) throughout the test even during softening. Therefore, the drained test (that uses a different set of control variables) can remain stable in a strain hardening regime although there is obviously a latent instability present that can be triggered by a change of control conditions.

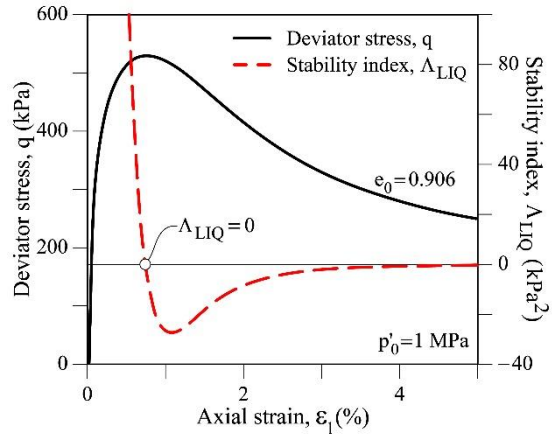

a)

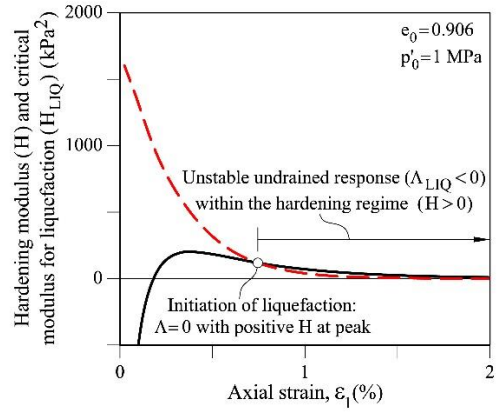

b)

Figure 13. MIT-S1 simulations of loose Toyoura sand (modified from Buscarnera and Whittle 2013): a) evolution of deviator stress and stability index; b) evolution of hardening modulus and critical modulus for liquefaction

3 TRIGGERING FLOW LIQUEFACTION

If a loose material is deposited along a slope, liquefaction may occur with minimum disturbance if the inclination is large enough (e.g. di Prisco et al. 1995). This phenomenon probably corresponds to the concept of 'spontaneous liquefaction' introduced by Terzaghi (1957). However, in other circumstances, a triggering

event is required to set off liquefaction. Consider for instance the undrained stress path of a specimen of a flow liquefaction-prone material after Ko consolidation (Figure 14a). It is necessary to apply an additional deviator stress to reach peak strength and start the softening regime. The additional deviator may arise from an undrained increase in vertical stress (total stress path A), a reduction in horizontal stress (total stress path B) or a combination of the two. It should be noted that, in terms of effective stress paths, the different undrained loading types are all equivalent. A drained lateral stress reduction may also lead to instability and liquefaction (Figure 14 b). Liquefaction can also be triggered by an increase of pore pressure that may be due to changes in hydraulic conditions (Figure 14 c) or to the effects of cyclic loading (Figure 14d). The latter case should not be confused with cyclic liquefaction. In all the three latter cases (14b, c, d), soil behaviour becomes undrained once the instability point has been reached.

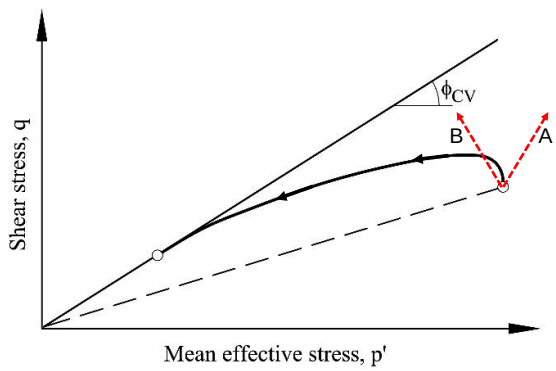

a)

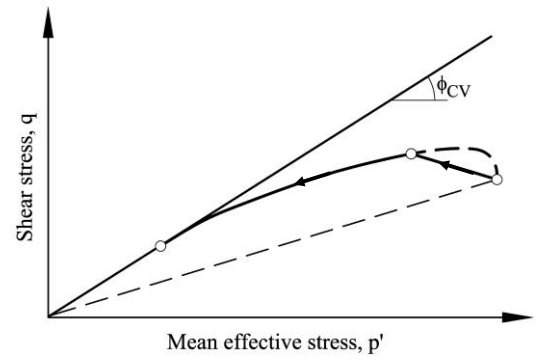

b)

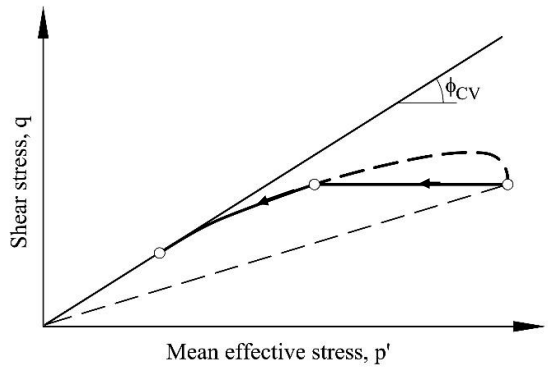

c)

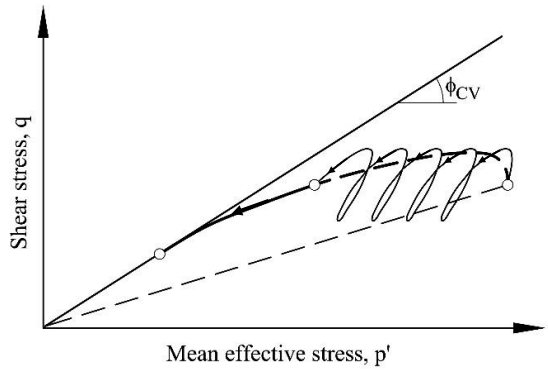

d)

Figure 14. Triggering mechanisms for flow liquefaction: a) undrained increment of deviator stress; b) drained unloading; c) pore pressure increase due to change in hydraulic conditions; d) pore pressure increase due to cyclic loading

A number of different physical triggering mechanisms for flow liquefactions have been identified (e.g. Martin and Mc Roberts 1999). They can be classified in the following manner:

a) Load increase due to emplacement of the material or other construction activities on the surface. The placing of the material cannot be uniform as Ko conditions, by definition, will never lead to static failure. (Figure 14 a, path A).

b) Lateral stress reduction due to foundation sliding, dam overtopping, toe erosion or excavation. In this unloading case, triggering may be undrained if those events are rapid (Figure 14a, path B) or drained if they occur very gradually (Figure 14b).

c) Changes in pore pressures due to increased pond levels, unfavourable weather conditions or pore pressure redistribution (Figure 14c).

d) Vibrational loads due to earthquakes, construction traffic or blasting (Figure 14 d).

Lateral stress reduction due to basal sliding is a very common trigger of flow liquefaction. It has been identified in the cases of Fort Peck Dam, Mount Polley dam, Kingston fly ash dike and Fundão dam. In the failure of Aberfan spoil tip, the immediate cause was also a sliding on a pre-existing shear surface that triggered the liquefaction of the colliery waste that had been taken close to saturation by rainfall. In Merriespruit dam, the lateral stress release was brought about by overtopping and rapid erosion of the dam. In the well-known case of Lower San Fernando dam, the triggering mechanism was not foundation failure and lateral stress reduction but the increase of pore pressures that resulted from the redistribution of pore pressures set up during the preceding earthquake.

4 ANALYSIS OF THE CPTU TEST IN UNDRAINED SOFTENING MATERIALS

4.1 General

It is difficult to extract really undisturbed samples from most materials that are prone to flow liquefaction (clean sands, silty sands, sandy silts and silts). For this reason, soil characterization is usually based on in situ tests (Viana da Fonseca 2013); currently, cone penetration tests (CPT and CPTu) are probably the most dominant ones. Normalized parameters based on cone penetration records have been used as a screening tool to assess whether a particular soil deposit is potentially flow-liquefiable. The most commonly used ones are:

$$Q_t = (q_t - \sigma_{vo}) / \sigma'_{vo} \tag{6}$$

$$F = f_s / (q_t - \sigma_{vo}) \tag{7}$$

$$B_q = (u_2 - u_o) / (q_t - \sigma_{vo}) \tag{8}$$

$$Q(1 - B_q) + 1 = (q_t - u_2) / \sigma'_{vo} \tag{9}$$

where q_t is the total cone penetration resistance, u_2 is the pore pressure measured at the shoulder of the cone in CPTu tests, u_0 is the initial pore pressure, and σ'_{v0} and σ_{v0} are the initial effective and total vertical stresses respectively.

Thus, Robertson (1990, 2009. 2010a, 2012, 2016) used a Q_t - F space to map regions of different soil type behaviour; potential flow liquefaction is associated materials with contractive behaviour. Alternatively, the potential for flow liquefaction can be evaluated by determining the state parameter,ψ, from the cone penetration data (Been et al. 1986, 1987, Jefferies and Been 2006, Robertson 2010b, Reid 2015, Been 2016). The relationship between the state parameter and cone penetration resistance is not however unique but it is affected by a number of other soil properties that, ideally, should be

taken into account (Shuttle and Jefferies 1998). The availability of G_0, independently measured with the seismic cone, can provide additional useful information for a more accurate estimation of the state parameter (Schnaid and Yu 2007).

Undrained shear strength at the critical state (normalised by the initial effective vertical stress) have been estimated from backanalysed case histories (Olson and Stark 2002, Robertson 2010). They fall in the range of 0.05 to 0.15. Empirical relationships have been developed relating those strength values (sometimes supplemented with laboratory test results) with cone penetration data (Yoshimini et al. 1999, Robertson 2010). The evaluation depends strongly on the specific value of the soil behaviour type (SBT) leading to some significant uncertainty. Critical state undrained strength can also be derived from the value of the state parameter (Jefferies and Been 2006); in this case, uncertainties arise from the method of state parameter estimation.

In any case, interpretation of the cone penetration test is difficult and a satisfactory outcome would ideally require the combination of physical tests (calibration chambers or centrifuges), case histories and numerical analyses. There are a significant number of calibration chamber results but they are usually limited to clean sands leaving unexplored the important case of silts and silty materials. Interpretation of case histories is always approximate because relevant information is often missing or incomplete.

The challenges for the numerical analysis of cone penetration are considerable. Shuttle and Jefferies (1998) and Shuttle and Cunning (2007) have performed large deformation analysis assimilating cone penetration to a spherical cavity expansion but, obviously, this approach, while providing important insights, can only be considered a first approximation. A more realistic simulation of cone penetration requires the incorporation of the actual geometry and dealing with the nonlinearities associated with large deformations, appropriate soil constitutive models and cone/soil interface characteristics. Advanced numerical procedures currently exist that allow the performance of such analyses with a reasonable degree of success. Examples are the various formulations of Arbitrary Lagrangian-Eulerian procedures (ALE) (Wang et al. 2015) such as the Remeshing and Interpolation Technique by Small Strain (RITSS) (Zhou and Randolph 2009), the efficient ALE (EALE) approach (Nazem et al. 2006) and the Coupled Eulerian-Lagrangian (CEL) method (Pucker et al. 2013). Other possibilities are the Material Point Method (MPM) (Solowski and Sloan 2015) or the Particle Finite Element Method (PFEM) (Oñate et al. 2004, Zhang et al. 2028). Applications of those methods to the cone penetration test have been reported in a number of cases (e.g. Lu et al. 2004, Nazem et al. 2012, Walker and Yu 2006, Ceccato et al. 2016, 2017, Gens et al. 2016, Monforte et al. 2017a, 2018) although they do not address the case of undrained softening.

In this section, selected results of numerical analyses of the cone penetration test in an undrained softening material are presented. They are part of a systematic exploration of the effects of brittleness on the interpretation of the cone penetration test, currently under way.

4.2 Features of the PFEM analyses

The CPTu test has been analysed using the PFEM to examine the effect of increasing brittleness on the results of the cone penetration test. A coupled PFEM formulation (Monforte et al. 2017b, 2018) has been used in order to obtain not only the total cone resistance but also the pore pressure field developed during penetration. The PFEM can be summarised in the following points:

- The nodes of the domain of analysis are treated as particles whose motion is tracked during the solution process
- The particles are used as nodes of a Finite Element mesh.

- The FE discretization is periodically re-meshed (h-adaptive techniques are used) by Delauney tessellation, new nodes are included if necessary, and element smoothing is performed
- The continuum is modelled using an Updated Lagrangian formulation
- Interpolation algorithms are applied to transfer information between successive meshes
- Although it is not strictly required, well-shaped low order elements are used

The computational procedure sequence is illustrated in Figure 15.

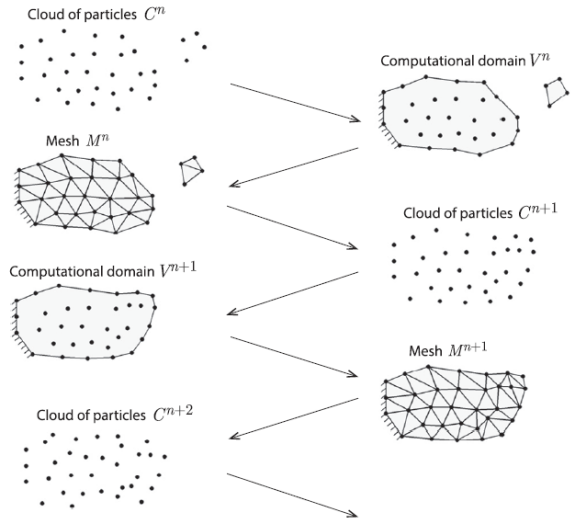

Figure 15. Scheme of a PFEM analysis

However, because the simulation of flow-liquefiable materials requires the representation of undrained softening, an additonal important development is required. It is well-known that conventional finite element analyses of softening materials rend to deliver non-objective results that exhibit a pathological dependence on mesh size (Bazant and Pijaudier-Cabot 1988, De Borst et al. 1993). In order to obtain correct results, it is necessary to use one of a number of existing regularization techniques (Bazant and Jirasek 2002). For these analyses, a non-local formulation (Manica et al. 2018) based on the weighting function of Galavi and Schweiger (2010) has been incorporated into the PFEM procedure. The essence of the formulation is the assumption that the state of a particle point depends not only on the variables of the point itself but also on the variables of neighbouring points (Figure 16).

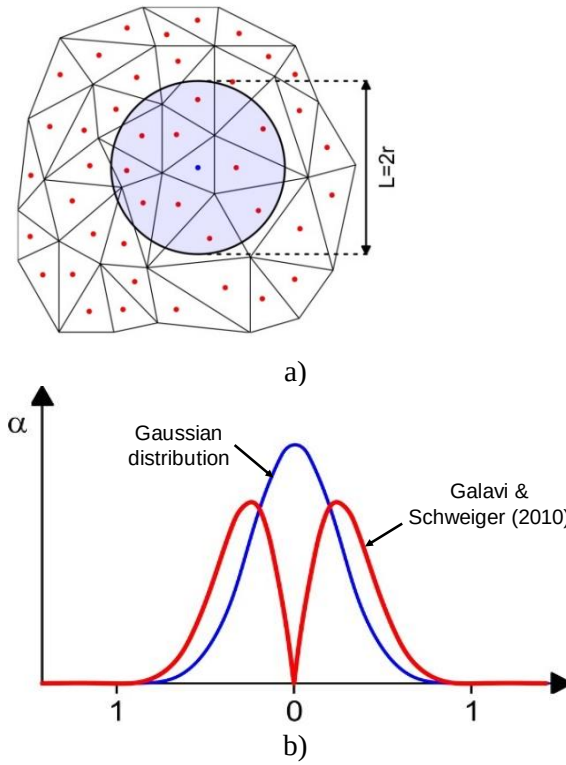

Figure 16. a) Stress points considered in the neighbourhood of a point in a nonlocal formulation; b) Weighting functions

4.3 Constitutive model

There are significant number of constitutive models available that are capable of simulating the undrained softening that underlie flow liquefaction phenomena (e.g. Jefferies 1993, Manzari and Dafalias 1997, Yu 1998, Pestana and Whittle 1999, Gajo and Muir Wood 1999, Imam et al. 2005). Most are isotropic but the MIT–S1 model can account for anisotropic

behaviour (Pestana et al. 2002). In the analyses presented here, a somewhat modified version of the CASM model (Yu 1998) has been used and is briefly presented here. The CASM model has been selected because i) it is relatively simple having a single yield surface, ii) it is based on the state parameter concept, iii) it uses non-associated plasticity allowing for instability phenomena to be reproduced, and iv) selecting appropriate parameters, it can mimic classical critical state models. Naturally, there are shortcomings associated with simplicity: the model is isotropic and the simulated behaviour inside the yield surface is quite simplistic. It has sufficient flexibility, however, to model a range of behaviour spanning from loose to dense states, including, naturally, the softening behaviour underlying flow liquefaction.

A schematic summary of the model is presented in Figure 17 where the concept of state parameter, ξ, is illustrated. The reference state parameter, ξ_r, defines the spacing, r, between the reference consolidation line and the critical state line, CSL. The model is based on a general expression for the state boundary surface of the following form:

$$\left(\frac{\eta}{M}\right)^n = 1 - \frac{\xi}{\xi_r} \tag{10}$$

where η is the stress ratio (q/p'), M is the slope of the CSL in q-p' space and n is a model parameter.

From geometrical considerations (Figure 17):

$$\frac{\xi}{\xi_r} = 1 + \frac{\ln(p'/p'_0)}{\ln r} \quad ; \quad r = \frac{p'_0}{p'_x} \tag{11}$$

and the following expression for the state boundary surface results:

$$\left(\frac{\eta}{M}\right)^n = -\frac{\ln(p'/p'_0)}{\ln r} \tag{12}$$

Through the variation of n and r, a wide variety of yield surface shapes can be obtained making the model very suitable for application to a wide range of materials.

The original CAM model used Rowe's dilatancy rule for the plastic potential but for the applications reported here, the following flow rule has been preferred (Yu 2006, Gonzalez 2011):

$$\frac{d\varepsilon_v^p}{d\varepsilon_q^p} = \frac{M^n - \eta^n}{m\eta^{n-1}} \tag{13}$$

where $d\varepsilon_v^p$ and $d\varepsilon_q^p$ are plastic volumetric and shear strains respectively and m is a parameter that controls the value of Ko for normally consolidated states. It can be noted that when η=M (critical state), dilatancy is zero. The hardening law is the classical isotropic volumetric strain rule of critical state soil models.

Often, it is required that the model is defined in terms of the undrained shear strength, $(s_u)_{SS}$ at critical (steady) state conditions. In that case, parameter r is expressed as (Gonzalez 2011):

$$r = \left(\frac{M}{2}\frac{p_e'}{(s_u)_{SS}}\right)^{\frac{1}{\Lambda}} \tag{14}$$

where p_e' is the equivalent pressure and Λ= (1-κ/λ) (Figure 17).

Figure 18 shows the capability of the model for simulating dense and loose behaviour under undrained conditions. More details on the model is given in Yu (1998, 2006) and Gonzalez (2011). It should be pointed out that, in this model, the undrained softening behaviour takes place under strain hardening conditions as discussed in section 2.5.

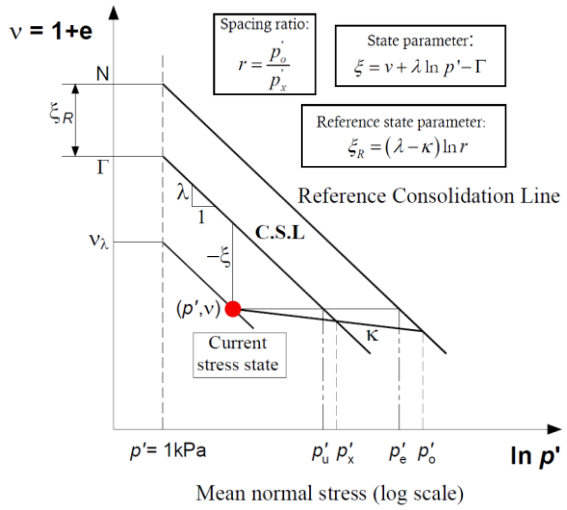

Figure 17. Definition of the CASM model (modified from Yu (1998)

4.4 Results

As indicated above, a systematic exploration of the effects of brittleness on the interpretation of the cone penetration tests is currently under way, only some illustrative results are shown here. For the set of analyses selected, appropriate values of *n* and *r* have been chosen in order to obtain the series of undrained stress paths and stress-strain curves of Figure 19. It can be observed that the undrained peak strength is the same in all cases but the degree of brittleness varies. Case A exhibits the lowest critical state undrained shear strength and, consequently, the maximum brittleness whereas case G corresponds to the minimum degree of brittleness.

The geometry and boundary conditions of the analyses are shown in Figure 20. The cone is pushed into the soil at the standard rate of 2 cm/s. Because of the low permeability adopted for the soil (a silty material has been assumed), penetration is basically undrained. The initial effective vertical and horizontal stresses are 96 kPa and 56 kPa, respectively, i.e. a Ko value of 0.58 has been assumed. Note that, because of the CASM model formulation, all results of the analyses can be normalized by the value of initial effective stresses.

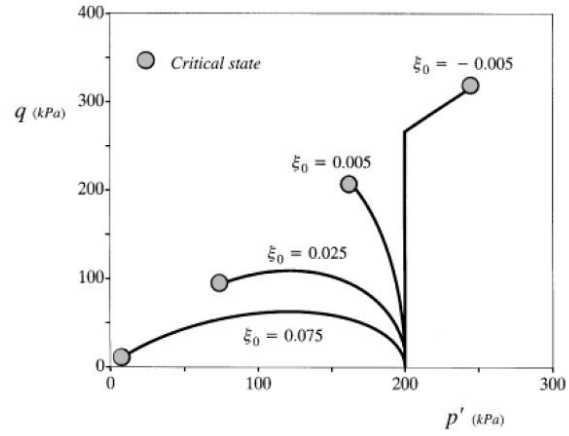

a)

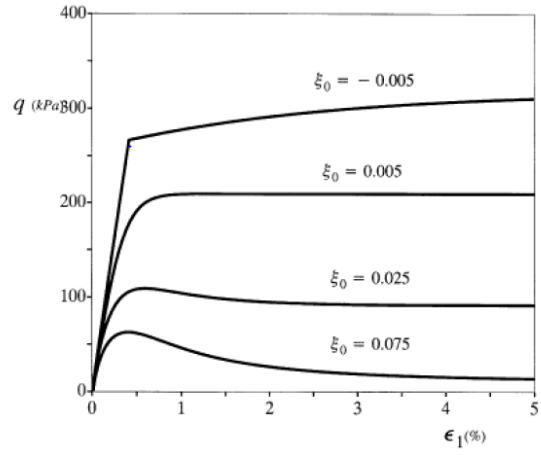

b)

Figure 18. Range of soil behaviour simulated by the CASM model (Yu 1998). Effect of state parameter in an undrained triaxial test: a) effective stress path; b) stress-strain curves

Figure 21 shows the results of the analyses in terms of net cone resistance (q_n), i.e. the total cone resistance minus the total vertical stress, the excess pore pressure at the cone face (Δu_1) and the excess pore pressure measured at the cone shoulder (Δu_2) whereas Figure 22 shows the same results in terms of the normalised parameters Q_t, B_q and $Q_t(1- B_q)+1$. As expected, although all the cases have the same peak undrained shear strength, the degree of brittleness has a very

strong influence on the results. This is illustrated in Figure 23 where Q_t, and B_q are plotted against Bishop's brittleness index. The effect of brittleness on the development of pore pressures is apparent in Figure 24 where the pore pressures around the cone (normalised by the net cone resistance) are compared for cases A (maximum brittleness) and G (minimum brittleness).

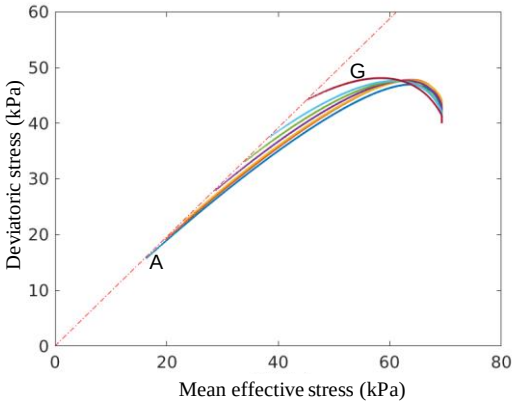

a)

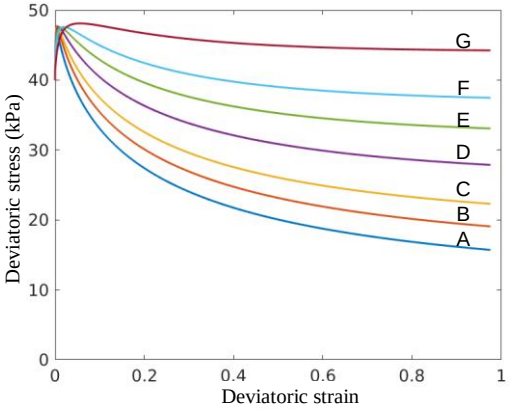

b)

Figure 19. Simulated soil behaviour for the analyses of the CPTu test: a) effective stress path; b) stress-strain curves

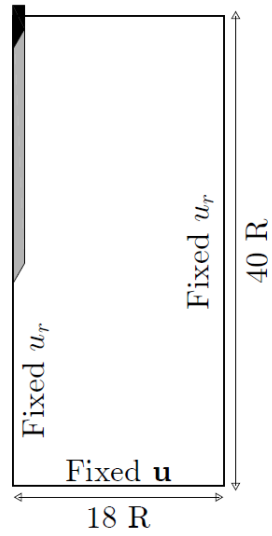

Figure 20. Analysis of the CPTu test. Geometry and boundary conditions

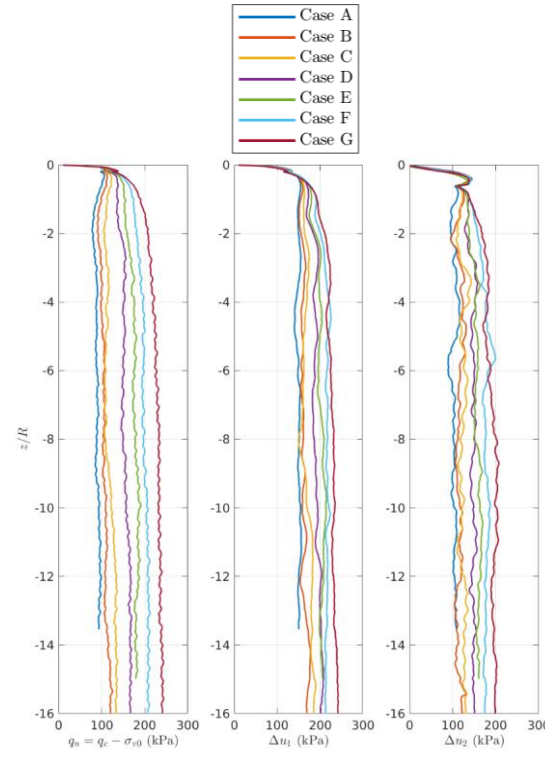

Figure 21. Results of the simulations of the CPTu test: net cone resistance (q_n), excess pore pressure at the cone face (Δu_1) and excess pore pressure at the cone shoulder (Δu_2)

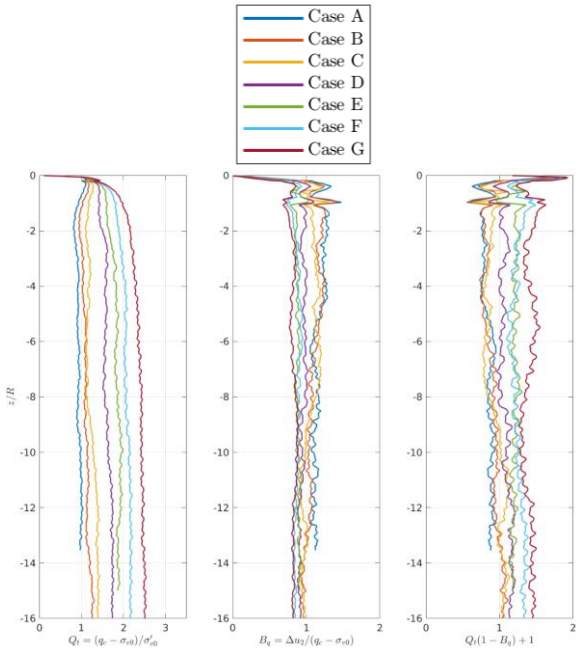

Figure 22. Results of the simulations of the CPTu test in terms of the normalised parameters Q_t, B_q and $Q_t(1-B_q)+1$.

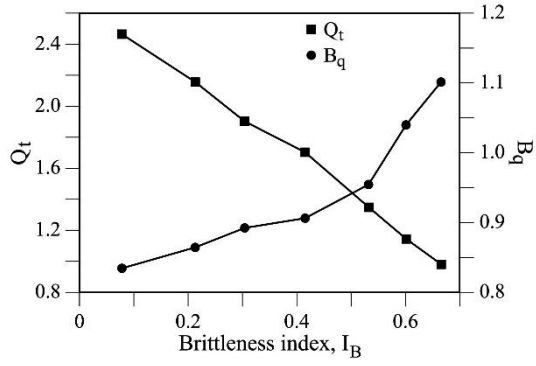

Figure 23. Variation of normalized parameters Q_t, and B_q with brittleness index

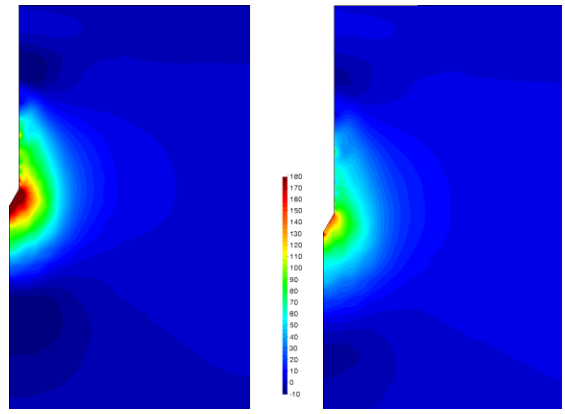

a) b)

Figure 24. Contours of pore pressures (normalised by the net cone resistance): a) case A, maximum brittleness; b) case G, minimum brittlenes

5 CASE HISTORY 1: AZNALCOLLAR DAM

Aznalcóllar tailings dam failed catastrophically in April 1998 (Figure 25) when the top of the dam had reached a height of 28 m above foundation level. The case has been described in detail in Alonso and Gens (2006a) and Gens and Alonso (2006b). In this instance, tailings were not used to form the retaining structure but a rockfill dam with an upstream clay blanket was designed and built. The dam failed by sliding on the foundation; the failure surface was located in the blue Guadalquivir clay that underlie the site. Figure 26 shows the mechanism of failure. The foundation clay exhibited the classical brittle behaviour associated with many stiff clays that led to the development of progressive failure. Failure resulted in a maximum quasi-horizontal displacement of over 50 meters. The dam and the upper part of the foundation moved downstream as a rigid body. This large movement allowed the opening of a breach in the dam that in turn made possible the spillage of water and tailings. Water and tailings caused the visible erosion of the dam that allowed more material to be released into the

environment. In total, it is estimated that the 7 million m^3 spillage was composed of 5.5 million m^3 of contaminated water, 1.3 million m^3 of tailings and 0.2 million m^3 of dam materials. Tailings were mainly dragged away by water erosion, most of the tailings remained inside the basin because they had a small degree of cementation and therefore a modest amount of cohesion. There were no casualties due to the failure but the environment damage was enormous. Acording to the multi-criteria ranking used by the worldminetailingsfailures.org. website, the Azanalcóllar failure is one of the twenty worst mine tailings disasters in history.

Figure 25. View of Aznalcóllar dam after failure

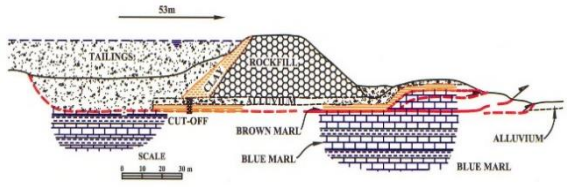

Figure 26. Mechanism of failure

The tailings had been deposited hydraulically in the lagoon; the material involved in the sliding failure were silt-size pyrite tailings. Coarser materials (pyroclastic tailings) had been deposited in the adjacent basin but they were not involved in the foundation failure. The pyrite tailings had a quite uniform grading (average D_{50}: 10 microns). The material was non-plastic, with high density (3-3.3 g/cm^3), a high friction angle (around 40º) and low permeability (about 10^{-6} - 10^{-7} m/s). There was clear evidence after the failure that the tailings close to the failed section of the dam had undergone liquefaction (Figure 27). However, the liquefaction of the tailings was not the cause of the failure but a consequence. When the dam started to move on the slip surface, lateral stress reduced and deviatoric stress increased so that the undrained stress path went over the peak strength (similarly to stress path B in Figure 14a). Liquefaction followed from that moment on.

Figure 27. Evidence of tailings liquefaction

The study of the dynamics of the failure of Aznalcóllar dam was reported in Alonso and Gens (2006b). Because of the simple failure mechanism involved, it was possible to represent realistically the problem as a rigid body motion of the dam and upper part of the foundation materials (Figure 28). The moving body (mass M) is subjected to thrust (F_T) and resisting (F_R) forces. If they are not in equilibrium, an acceleration, a, will result (equation 15).

$$\sum F = \sum F_T + \sum F_R = Ma \qquad (15)$$

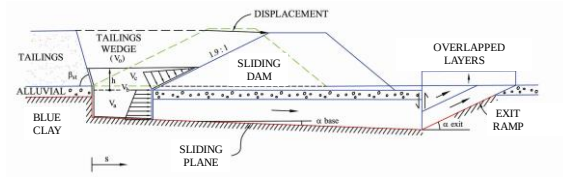

Figure 28. Scheme of the motion analysis of Aznalcóllar dam slide (Alonso and Gens 2006b)

The thrust force F_T is exerted by the tailings whereas there are two main components of the resisting forces, the friction along the sliding force F_{RF} and the passive resistance of the ground at the toe of the dam, F_{RF}. If the acceleration is computed using equation (16), a single integration in time provides the velocity of the dam and a double integration, the displacement.

$$\sum F = F_T + \left(F_{RF} + F_{RP}\right) = M\,\frac{d^2x}{dt^2} \qquad (16)$$

It has proved possible to make quite reasonable estimates of those forces and their variation with dam displacement (Alonso and Gens 2006b). The results are shown in Figure 29. It can be noted that the base resistance of the sliding plane reduces because the strength of the blue clay is decreasing towards the residual value. In contrast, the passive resistance provided by the ground at the toe of the dam increases because the sediments located there rise as a consequence of the movement of the dam. However, the most important contribution to the failure dynamics is provided by the tailings. Once they liquefy (due to the initial movement of the dam), they provide a very large additional thrust that is decisive for increasing drastically the acceleration of the dam and, consequently, the velocity and final displacement. Tailings also provide the braking mechanism because they fill the volume left by the sliding mass, their height reduces and their thrust diminishes accordingly. The variation of the resulting force with time is also plotted in Figure 29.

The resulting evolutions of velocity and displacement are plotted in Figure 30. It can be seen that the computed total displacement is of the same order as that observed in the field. The duration of the motion is 15.5 s, the maximum speed 5.5 m/s and the maximum computed acceleration 0.14g. Unfortunately, the only observations available are the final displacements of the dam; the failure occurred at about 2:30 in the morning and there were no eyewitnesses. Although computations included a number of uncertain variables, sensitivity analyses showed that the final outcome of the calculations was very robust with only modest variations in the computed final dam displacement.

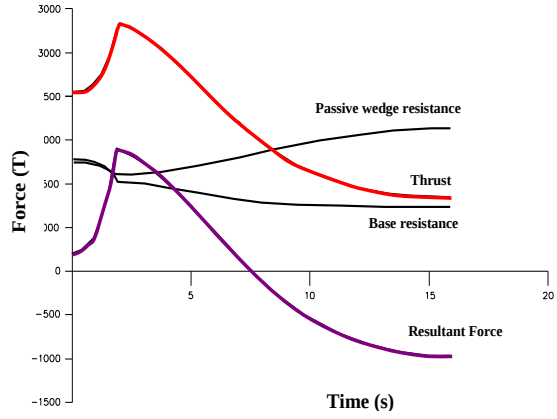

Figure 29. Variation of thrust, resistance and resultant forces with time

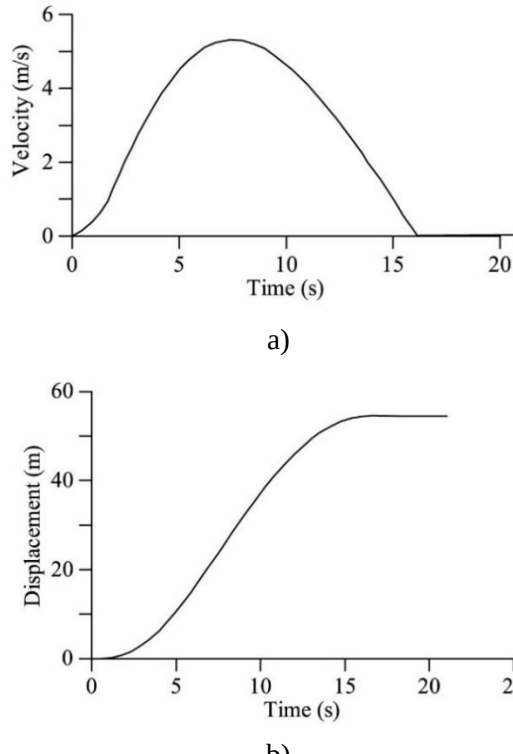

Figure 30. a) Evolution of dam velocity with time; b) evolution of dam displacement with time

6 CASE HISTORY 2: PRAT QUAY

6.1 Background

Prat quay provides the platform for a new container terminal, part of the latest development of Barcelona Harbour. It has a total length of 1,580 m and its construction was divided in two phases, Phase 1, 1000 m long, and Phase 2, 580 m long. Caissons were used to construct the quay wall; 25 units for Phase 1 and 12 for Phase 2 (Figure 31). On January 1st 2007, the Phase 1 quay wall failed catastrophically over a length of 600 m (Figures 32 and 33). Figure 34 shows the distanced travelled by the 15 caissons involved in the failure. It can be observed that some of the caissons travelled long distances, up to 90 m in one case.

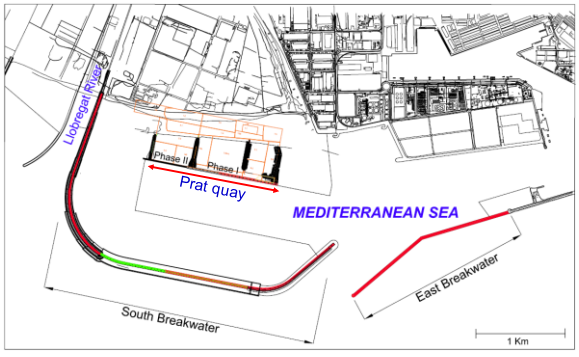

Figure 31. Location of the Prat quay

Figure 32. View of the Prat quay failed section

Figure 33. Length of the Prat quay failure and maximum distance travelled by the caissons

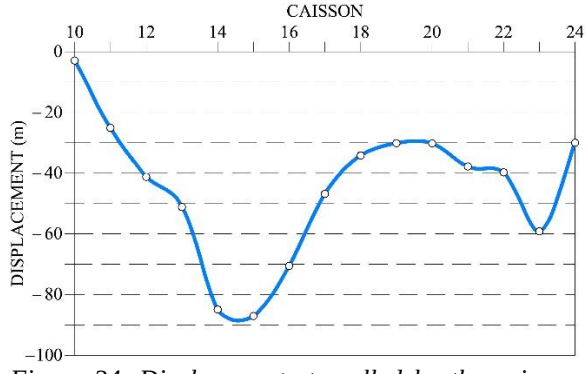

Figure 34. Displacements travelled by the caissons involved in the failure

The process of construction was as follows: i) dredging of the natural soil from an elevation of approximately -8.0 m to elevation -25.0 m, ii) construction of a rubble mound to elevation -16 m, iii) emplacement of the caisson on the rubble mound, iv) filling of the caisson cells with sand, and v) placement of the hydraulic fill at the back of the caissons. Hydraulic backfill was placed by rainbowing (Figure 1). The quay wall and the hydraulic backfill sit on the natural ground that, in this particular area, is made up of soft silty clay down to depths of 60-70 m below sea level.

The state of the quay at the moment of failure is illustrated in Figure 35. The caisson is 17.5 m high (emerging 1.5 m above mean sea level) and 18.5 m wide. The width of the caisson is larger than in most designs, the reason being that the caisson was designed to withstand storm forces

while the South breakwater (Figure 31) was being completed. In addition, at the time of failure, two embankments were being constructed (South and East embankments, see Figure 33) on top of the the backfill. The aim was to isolate an area for preloading. The embankments were constructed by simply dumping rockfill on the hydraulic backfill.

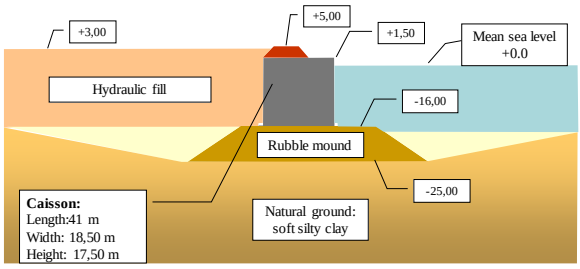

Figure 35. Cross-section of the Part quay before failure

Prior to failure, a 3.5 m high bund had been constructed on top of the caisson in order to allow the construction of the backfill to a higher elevation with the aim of accelerating preloading and reducing construction time. Naturally, this increased the pressures on the caisson wall. Backfill was rapid, it started in May 2006 and it was largely completed at the time of failure, eight months later. Failure occurred when the hydraulic backfill had reached an elevation of approximately +3.00 m and the water level behind the caissons an elevation of +3.50 m. At the moment of failure, the only site activity was hydraulic backfilling close to the area that failed.

Investigations after the failure clearly revealed that the underlying natural soft silty clay had not been involved. The rubble mound was in place and largely intact with perhaps only a small local failure at the seaward edge. Caisson sliding on the rubble mound was evidently the failure mechanism. The hydraulic fill liquefied and provided the necessary thrust to move the caissons the large distances observed. The largest movements were centred on caissons 14 and 15 close to the centreline of the South embankment. After investigation, it is strongly suspected that failure of the South embankment started the backfill liquefaction that subsequently spread to other locations. The failure could well have been triggered by release of air trapped in the backfill (Hight 2007); an eyewitness reported five or six air discharges in the relevant area minutes before the failure.

The fill involved in the failure had flowed and dispersed widely in the basin and therefore it was not available for investigation. The knowledge on the state and properties of the hydraulic fill before the failure has been based on the information provided by the remaining fill in Phase 1 and the fill in Phase 2 that had been placed in exactly the same way. The grading of a hydraulic fill is generally dependent on the location of a particular area with respect to the discharge point and on the distance that the soil particles have travelled before sedimentation. Therefore, it is not surprising that there was quite a significant span in the grading of the fill ranging from silty sands to clayey silts. In any case, the proportion of fines was generally high. Figure 36 shows an example of the particle size distributions obtained from the samples recovered from a particular borehole.

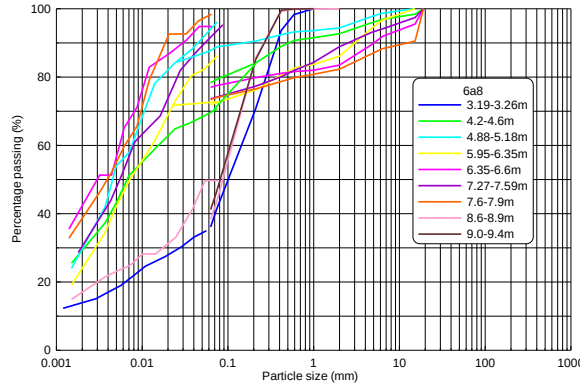

Figure 36. Particle size distributions from samples recovered from borehole 6a8.

A large campaign of CPTu tests was performed in both the failed and non-failed sections of the Prat quay covering both land and sea sides. Figure 37 shows the CPTu results in an unfailed section of Phase 1 on the land side. It is

apparent that the cone resistances are very small in the hydraulic fill, the transition to the natural ground clearly visible in most cases. It cannot be discarded that some excess pore water pressures were present in backfill areas of lower permeability. Figure 38 shows in more detail the CPTu observations of cone resistance, pore pressure and sleeve friction for a particular sounding. In Figure 39, the observations in the hydraulic fill of two representative CPTu tests are plotted in the SBT (soil behaviour type) charts proposed by Robertson (2016). It can be noted that there is a significant spread from sand-like to clay-like materials but practically all points indicate contractive behaviour and therefore with a potential for flow liquefaction.

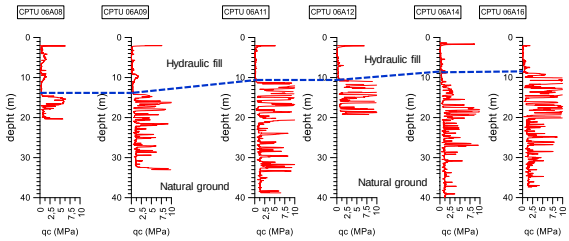

Figure 37. Cone resistance in a non-failed section of Phase 1

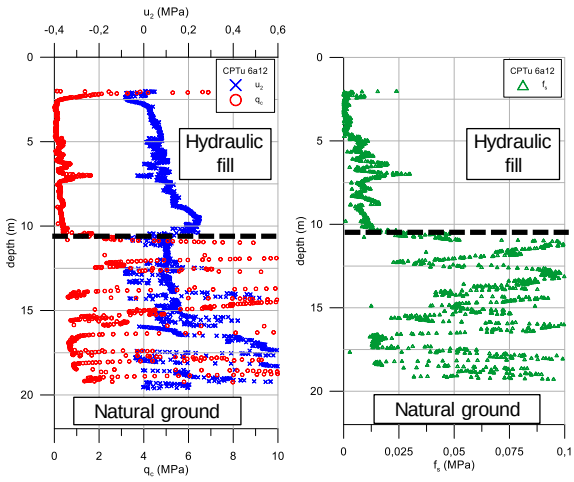

Figure 38. CPTu results of sounding 6a12

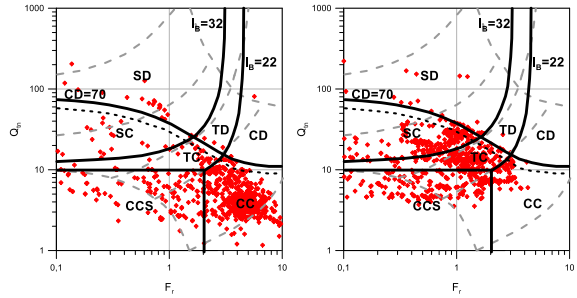

Figure 39. Location of the observations in two CPTu tests in Robertson (2016) SBT charts: a) CPTu 6a12 (Phase 1); b) CPTu 3b11 (Phase 2)

6.2 Analysis of failure

Ideally, a proper understanding of the failure and failure mechanism, including flow liquefaction, should be demonstrated by the performance of an analysis (Shuttle 2016) that, while incorporating the basic features of the case and of the behaviour of the materials involved, it proves capable of reproducing field observations and the failure characteristics in an adequate manner. In this particular case, a plane-strain numerical analysis has been performed simulating the history of construction up to the moment of failure. The behaviour of the hydraulic fill has been modelled using the CASM constitutive law in the manner described in section 4. Figure 40 shows the computed construction settlements compared with the observed settlements of all Phase 1 caissons. The agreement is quite satisfactory. Full details of the numerical analysis performed are provided in Tarragó (2019).

The triggering of the failure was simulated by assuming that a limited area of the backfill in the area of the South embankment and close to the surface liquefied. In that case, on reaching a backfill elevation of +3.0 m, the numerical analyses predicted failure with the mechanism shown in Figure 41, i.e. the caisson sliding on the rubble mound due to the backfill pressure. The development of failure after the initial liquefaction is clearly illustrated in Figure 42. It can be observed how the displacements associated with failure spread from the initial

liquefaction region until producing the complete failure of the caisson wall.

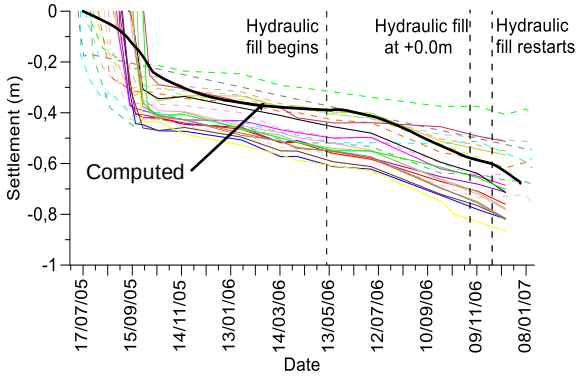

Figure 40. Caisson settlements before failure. Computed results vs. observations

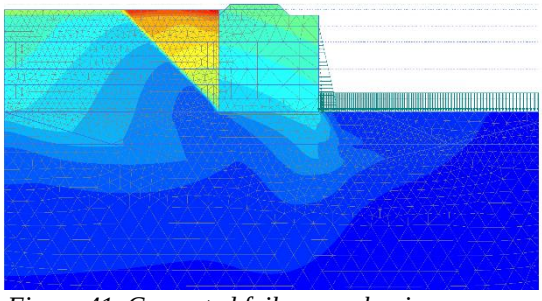

Figure 41. Computed failure mechanism

The subsequent development of caisson movements cannot be modelled with a conventional finite element analysis, a 3D PFEM analysis was performed (Celigueta et al. 2007). Because of the much larger complexity of the model (Figure 43), a simplified constitutive model had to be used where the strength drop was instantaneous coupled to an established rate of liquefaction propagation. Several hypothesis of liquefaction initiation were tried. The only analysis that resulted in caisson displacements similar to those observed in the field was the case in which liquefaction was initiated close to the tip of the South embankment followed by a second liquefaction episode close to the East embankment (Figure 44). The final computed position of the caissons are shown in Figure 45. Figure 46 shows the development of the computed displacements of the caissons during the analysis. It can be seen that the final situation is achieved after 41 seconds. The observed displacements are also plotted for reference.

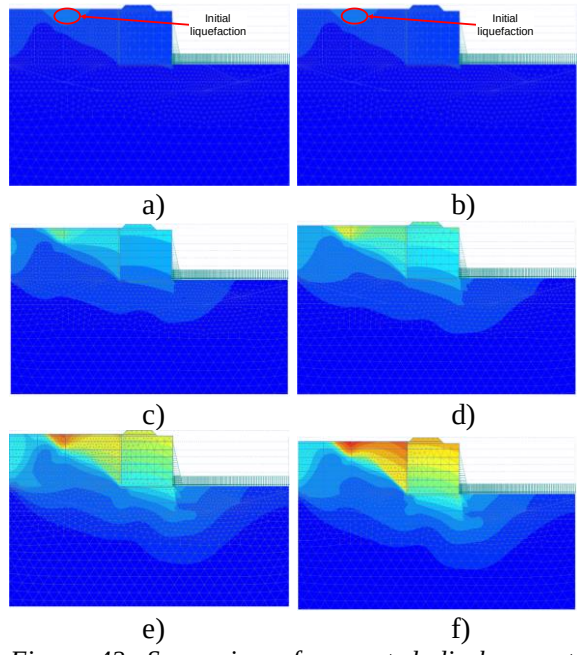

Figure 42. Succession of computed displacements contours during failure

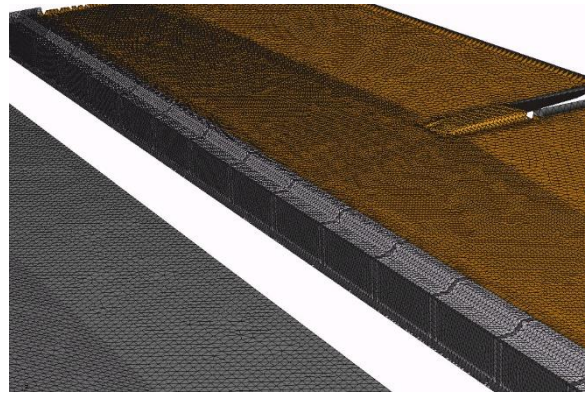

Figure 43. Mesh employed in the 3D PFEM analysis

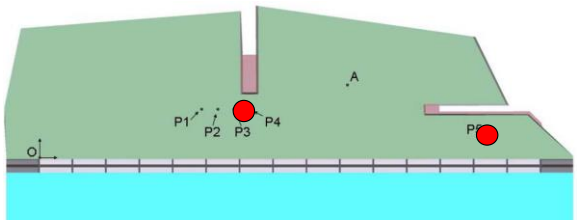

Figure 44. Assumed locations of succesive liquefaction initiation

Figure 45. Computed caisson locations at the end of failure from the PFEM analysis

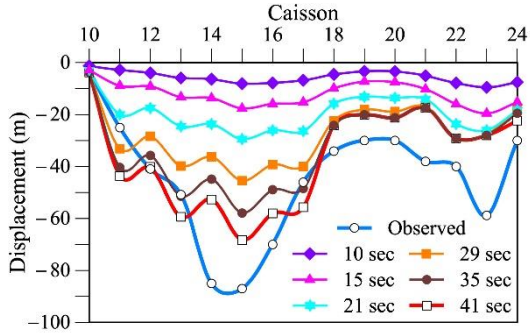

Figure 46. Evolution of computed caisson displacements with time. Observed caisson displacements are added for reference

The post-failure analysis appears to confirm that the initial liquefaction of the backfill was triggered by the failure of the south embankment. It also suggests that, when liquefaction reached the zone of the East embankment, an additional failure provided a new liquefaction focus. It should be noted however, that the analyses performed are necessarily quite simplified. Nevertheless, they appear capable of reproducing the basic traits of the post-failure phenomena.

In contrast to many previous cases, liquefaction of the hydraulic fill was not triggered in this instance by a conventional sliding failure underlying the site or by a pore pressure increase. On this occasion, it was the fill liquefaction that initiated the horizontal sliding of the caissons. Subsequently, the propagation of liquefaction and the associated loss of strength of a large amount of fill provided the unbalanced thrust force required to transport the large and heavy caissons considerable distances.

7 SUMMARY AND CONCLUDING REMARKS

Hydraulic fills are often deposited in a loose state making them susceptible to flow liquefaction, a phenomenon that has led to a number of catastrophic failures. Although some details are still uncertain, there is now a reasonable understanding of the fundamental mechanism of flow liquefaction grounded in a framework that incorporates the concepts of critical state and state parameter. Soils undergoing flow liquefaction exhibit undrained softening and therefore brittle behaviour. The conceptual framework allows distinguishing the very different character of peak strength and critical or steady state. New theoretical concepts such as that of controllability lead to a more rigorous definition of the undrained instability phenomena associated with flow liquefaction. A number of triggering factors exist that may lead to the onset of instability: additional loading, reduction of lateral stresses, increase of pore pressure, cyclic effects. They have all been documented in the literature although it seems that loss of lateral support is one of the most frequent triggering events.

Hydraulic fills and other materials prone to flow liquefaction are difficult to sample; they are usually characterized by means of in situ tests.

The CPTu test is one of the most commonly used ones. The interpretation of the CPTu test is generally of an empirical nature; the question arises, however, whether the information gathered mostly from conventional soils is readily applicable to materials that exhibit undrained softening. Some results of a systematic exploration of this issue by numerical analysis have been presented. The use of advanced numerical formulations are inevitably required to account for large deformations, highly nonlinear constitutive models and softening behaviour. The results demonstrate the large effect of the degree of brittleness on pore pressure response and, especially, on cone resistance.

Two case histories involving flow liquefaction of hydraulically deposited materials have been presented. The first one involved the failure of a tailings dam due to shear sliding of the foundation clay. In this case, liquefaction of the tailings was a consequence of the foundation failure; it was caused by the movement downstream of the dam reducing lateral support. However, analysis has demonstrated that tailings liquefaction was the prime cause of the catastrophic consequences of the failure. The additional thrust provide by liquefaction constituted the main driving force for the large displacements of the dam. In the absence of this additional thrust, a dam breach would not have opened and the catastrophic outcome would have been avoided.

The second case history concerns the failure of a harbour quay. In this case, the hydraulic fill liquefied before failure probably as a consequence of some construction activities on site. The initial liquefaction spread through the backfill causing the failure of the caisson wall without affecting the natural soil in the foundation. The unbalanced force resulting from the strength loss of the backfill was capable of moving the heavy caissons considerable distances, up to 90 m in one case. Analysis has been able to simulate quite satisfactorily the initial quay wall failure and the subsequent post-failure movements of the caissons.

It is evident that most hydraulic fills, like other brittle materials, constitute a serious potential risk on many occasions and that their use require especial caution. Failures due to liquefaction are generally unannounced and often have catastrophic consequences. In addition, there is a large variety of triggering events that can lead to liquefaction; some of them may prove difficult to prevent in practice. Naturally, there is a wide range of remedial measures that can be applied to reduce or eliminate the risk of liquefaction; indeed a number of them have been used in the reconstruction of the Part quay. Remediation measures are, however, outside the scope of this paper.

8 ACKNOWLEDGEMENTS

The paper has benefited from contributions of many colleagues. D. Tarragó has performed the analysis of the Prat quay failure as well as assisting in many other ways. L. Monforte undertook the complex task of the numerical computations of the CPTu tests. The assistance of M. Arroyo on various parts of the manuscript is also acknowledged. The investigations of Aznalcóllar dam and of the Prat quay failure were carried out jointly with E.E. Alonso. The involvement of A. Deu, J.L. Estrada, A. Soriano and J. Uzcanga in the Prat quay case is gratefully recognized. Special thanks are due to D.W. Hight for fruitful discussions on the Prat quay case. The post-failure analysis of the Prat quay failure was the work of M.A. Celigueta, E. Oñate, and B. Suárez. The support of the Barcelona Port Authority is also greatly appreciated.

9 REFERENCES

Alarcon-Guzman, A., Leonards, G.A., Chameau, J.L. 1988. Undrained monotonic and cyclic strength of sands. *Journal of Geotechnical Engineering, ASCE*, **114**, 1089–1110.

Alonso, E.E., Gens, A. 2006a. Aznalcóllar dam failure. Part 1: Field observations and

material properties, *Géotechnique* **56**, 165-183.

Alonso, E. E., Gens, A. 2006b. Aznalcóllar dam failure. Part 3: Dynamics of the motion, *Géotechnique* **56**, 203–210.

Andrade, J.E. 2009. A predictive framework for liquefaction instability, *Géotechnique* **59**, 673–682.

Bažant ZP, Jirásek M. 2002. Nonlocal integral formulations of plasticity and damage: survey of progress. *Journal Engineering Mechanics* **128**, 1119–1149.

Bažant, Z.P., Pijaudier-Cabot, G. 1988. continuum damage, localization instability and convergence. *Journal Applied Mechanics* **55**, 287–93.

Been, K. 2016. Characterizing mine tailings for geotechncial design. *Geotechnical and Geophysical Site Characterization 5* (Eds. Lehane, Acosta-Martínez, Kelly), 41-55. Australian Geomechanics Society, Sydney.

Been, K., Crooks, J.H.A., Becker, D.E, Jefferies M.G. 1986. The cone penetration test in sands: Part 1, State parameter interpretation. *Géotechnique* **36**, 239-249.

Been, K., Jefferies M.G., Crooks J.H.A., Rothenberg, L, 1987. The cone penetration test in sands: Part II, general inference of state. *Géotechnique* **37**, 285-299.

Been, K., Jefferies, M. G. 1985. A state parameter for sands. *Géotechnique* **35**, 99–112.

Been, K., Jefferies, M.G., Hachey, J. 1991. The critical state of sands, *Géotechnique* **41**, 365–381.

Bishop, A. W. 1973. The stability of tips and spoil heaps, *Quaterly Journal of Engineering Geology* **6**, 335–376.

Bishop A.W., Hutchinson, J.N., Perman, A.D.M., Evans, H.E. 1868. *Geotechnical Investigation into the Causes and Circumstances of the Disaster of 21st October , 1966*. A Selection of Technical Papers submitted to the Aberfan Tribunal, 1-80. Welsh Office, H.M.S.O., London.

Borja, R.I. 2006. Condition for liquefaction instability in fluid saturated granular soils, *Acta Geotechnica* **1**, 211–224.

Buscarnera, G., Dattola, G., and di Prisco, C. 2011. Controllability, uniqueness and existence of the incremental response: a mathematical criterion for elastoplastic constitutive laws. *International Journal of Solids and Structures* **48**, 1867–1878

Buscarnera, G., Whittle, A.J. 2013. Constitutive modelling approach for evaluating the triggering of flow slides, *Canadian Geotechnical Journal* **49**, 499–511.

Carrera, A., Coop, M.R., Lancellotta, R. 2011. The influence of grading on the mechanical behaviour of Stava tailings. *Géotechnique* **61**, 935–946.

Casagrande, A. 1936. Characteristics of cohesionless soils affecting the stability of earth fills. *J. Boston Society of Civil Engineers* **23**, 257–276.

Casagrande, A. 1965. Second Terzaghi lecture: role of the "calculated risk" in earthwork and foundation engineering. *Journal of the Soil Mechanics and Foundations Division, ASCE* **91**, 1-40.

Casagrande, A. (1975) Liquefaction and cyclic deformation of sands: A critical review. *Proceedings of the Fifth Pan-American Conference on Soil Mechanics and Foundation Engineering* **5**, 79-133. Buenos Aires, Argentina,

Castro, G. 1969. *Liquefaction of sands*. Harvard Soil Mechanics Series, No. 81. Cambridge, MA: Harvard University.

Castro, G., Keller, T.O., Boynton, S.S. 1989. *Re-evaluaiton of the Lower San Fernando Dam. An investigation of the February 9, 1971 slide*. Contract Report GL-89-2. US Army Corps of Engineers, Washington DC..

Ceccato, F., Beuth, L., Vermeer, P.A., Simonini, P. 2016. Two-phase Material Point Method applied to the study of cone penetration. *Computers and Geotechnics* **80**, 440-452.

Ceccato, F., Simonini, P. 2017. Numerical study of partially drained penetration and pore

pressure dissipation in piezocone test. *Acta Geotechnica* **12**, 195-209.

Celigueta, M.A., Oñate, E., Suárez, B. 2007. *Trabajos realizados por CIMNE en relación con la rotura del muelle del Prat del puerto de Barcelona (in Spanish)*. Informe Técnico, CIMNE IT-514. CIMNE, Barcelona.

Chandler R.J., Tosatti, G. 1985. The Stava tailings dams failure, Italy, Proceedings of the *Institution of Civil Engineers-Geotechnical Engineering* **113**, 67-79.

Ciantia, M.O., Arroyo, M., O'Sullivan, C., Gens, A., Liu T. 2019. Grading evolution and critical state in a discrete numerical model of Fontainebleau sand. *Géotechnique* **69**, 1-15.

Coop, M. 2015. Limitations of a Critical State Framework Applied to the Behaviour of Natural and "Transitional" Soils. *Advances in Soil Mechanics and Geotechnical Engineering* (Eds. Rinaldi, V.A., Zeballos, M.E., Claria, J.J.), 115-155. IOS Press, Amsterdam.

Darve, F., 1994. Liquefaction phenomenon: modelling, stability and uniqueness. *Verification of Numerical Procedures for the Analysis of Soil Liquefaction Problems.* (Eds: Arulanandan, K., Scott, R.F.), 1305–1319. Balkema, Rotterdam.

Davies, M., McRoberts, E., Martin, T. 2002. Static liquefaction of tailings – Fundamentals and case histories. *Tailings Dams 2002*. ASDSO/USCOLD, Las Vehgas, Nevada.

De Borst, R., Sluys, L.J., Mühlhaus, H.-B., Pamin, J. 1993. Fundamental issues in finite element analyses of localization of deformation. *Engineering Computations* **10**, 9–121

di Prisco, C., Matiotti, R., Nova, R. 1995. Theoretical investigation of the undrained stability of shallow submerged slopes. *Géotechnique* **45**, 479–496.

Fourie, A.B., Blight, G.E., Papageorgiou, G. 2001. Static liquefaction as a possible explanation for the Merriespruit tailings dam failure. *Canadian Geotechnical Journal* **38**, 707–719.

Fourie, A.B., Papageorgiou, G. 2001. Defining an appropriate steady state line for Merriespruit gold tailings. *Canadian Geotechnical Journal 38*, 695–706.

Fourie, A.B., Tshabalala, L. 2005. Initiation of static liquefaction and the role of K0 consolidation. *Canadian Geotechnical Journal* **42**, 892–906

Gajo, A., Muir Wood, D. (1999) Severn-Trent sand, a kinematic hardening constitutive model: The q-p formulation. *Géotechnique* **49**, 595- 614.

Galavi, V., Schweiger, H.F. 2010. Nonlocal multilaminate model for strain softening analysis. *Int. Journal of Geomechanics* **10**, 30–44

Gens, A. 1982. *Stress–strain and strength of a low plasticity clay*. Ph.D. Thesis. Imperial College, London.

Gens, A., Alonso, E. E., 2006. Aznalcóllar dam failure. Part 2: Stability conditions and failure mechanism, *Géotechnique* **56**, 185–201.

Gens, A., Arroyo, M., Butlanska, J., Carbonell, J.M Ciantia, M., Monforte, L., O'Sullivan, C. 2016. Simulation of the cone penetration test: discrete and continuum approaches, *Australian Geomechanics* **51**, 169-182.

González, N.A. 2011. *Development of a family of constitutive models for geotechnical applications.* Ph.D. Thesis. Universitat Politècnica de Catalunya, Barcelona.

Hight, D.W. 2002. Personal communication.

Hight, D.W., Georgiannou, V.N., Martin, P.L., Mundegar, A.K. 1999. Flow slides in micaceous sands. In *Proceedings of the International Symposium on Problematic Soils*, (Eds. Yanagisawa, E., Moroto, N. & Mitachi, T.), 945–958. Balkema, Rotterdam.

Hird, C.C., Hassona, F. 1990. Some factors affecting the liquefaction and flow of saturated sands in laboratory tests. *Engineering Geology* **28**, 149-170.

Imam, S.M.R., Morgenstern, N.R., Robertson, P.K., Chan D.H. 2005. A critical-state constitutive model for liquefiable sand.

Canadian Geotechnical Journal **42**, 830-855.

Imposimato, S., Nova, R. 1998. An investigation on the uniqueness of the incremental response of elastoplastic models for virgin sand, *Mechanics of Cohesive-Frictional Materials* **3**, 65–87.

Ishihara, K. 1993. Liquefaction and flow failure during earthquakes, *Géotechnique* **43**, 351–451.

Jefferies, M.G. 1993. Nor-Sand: a simple critical state model for sand, *Géotechnique* **43**, 91–103.

Jefferies, M.G., and Been, K. 2006. *Soil liquefaction: a critical state approach.* Taylor and Francis, New York.

Jefferies, M.G., and Been, K. 2016. *Soil liquefaction: a critical state approach (2nd edition).* Taylor and Francis, Boca Raton.

Konrad, J.-M. 1993. Undrained response of loosely compacted sands during monotonic and cyclic compression tests. *Géotechnique* **43**, 69–89.

Kuerbis, R.H., Vaid, Y.P. 1988. Sand sample preparation - The slurry deposition method. *Soils and Foundations* **28**, 107-118.

Lade, P.V. 1993. Initiation of static instability in the submarine Nerlerk berm. *Canadian Geotechnical Journal* **30**, 895–904.

Lade, P.V., Yamamuro, J.A. 1997. Effects of nonplastic fines on static liquefaction of sands. *Canadian Geotechnical Journal* **34**, 918-928.

Li, W., Coop, M.R., Senetakisc, K.,. Schnaid, F. 2018. The mechanics of a silt-sized gold tailing. *Engineering Geology* **241**, 97-108.

Lu, Q., Randolph, M.F., Hu, Y., Bugarski, I.C. 2004. A numerical study of cone penetration in clay, *Géotechnique* **54**, 257–67.

Manica, M., Gens, A., Vaunat, J., Ruiz, D.F. 2018. Nonlocal plasticity modelling of strain localisation in stiff clays. *Computers and Geotechnics* **103**, 138–150.

Manzari, M.T., Dafalias, Y.F. 1997. A critical state two-surface plasticity model for sands. *Géoteclmique* **47**, 255-272.

Martin, T.E., McRoberts E.C. 1998. Some considerations in the stability analysis of upstream tailings dams 287-302. *Tailings and Mine Waste '99*, Fort Collins, Colorado,

Monforte, L., Arroyo, M., Carbonell, J.M., Gens, A. 2018. Coupled effective stress analysis of insertion problems in geotechnics with the Particle Finite Element Method, *Computers and Geotechnics* **101**, 114–129.

Monforte, L., Arroyo, M., Carbonell, J.M., Gens, A. 2017a. Numerical simulation of undrained insertion problems in geotechnical engineering with the particle finite element method (PFEM), *Computers and Geotechnics* **82**, 44–156

Monforte, L., Carbonell, J.M., Arroyo, M., Gens, A. 2017b. Performance of mixed formulations for the particle finite element method in soil mechanics problems, *Computational Particle Mechanics* **4**, 269-284.

Morgenstern, N.R., Vick, S.G., Viotti, C.B., Watts, B.D. 2016. *Report on the Immediate Causes of the Failure of the Fundão Dam*. Fundão Tailings Dam Review Panel

Muir Wood, D. 2007. The magic of sands – the 20th Bjerrum Lecture presented in Oslo, 25 November 2005. *Canadian Geotechnical Journal 44*, 1329–1350.

Nazem, M., Sheng, D., Carter, J.P. 2006. Stress integration and mesh refinement for large deformation in geomechanics, *Int J Numer Meth Eng* **65**, 1002–1027.

Nazem, M., Carter, J.P., Airey, D.W., Chow, S.H. 2012. Dynamic analysis of a smooth penetrometer free-falling into uniform clay, *Géotechnique* **62**, 893–905.

Nicot, F., Darve, F., Khoa, H.D.V., 2007. Bifurcation and second-order work in geomaterials. *International Journal for Numerical and Analytical Methods in Geomechanics* **31**, 1007–1032.

Nova, R. 1989. Liquefaction, stability, bifurcations of soil via strainhardening plasticity. In *Numerical Methods for Localisations and Bifurcations of Granular*

Bodies, Proceedings of an International Workshop.(Eds. Dembicki, E., Gudehus, G. & Sikora Z.), 117–132. Technical University of Gdansk, Gdansk

Nova, R. 1994. Controllability of the incremental response of soil specimens subjected to arbitrary loading programmes, *Journal of the Mechanical Behavior of Materials* **5**, 193–202.

Olson, S. M., and Stark, T. D. 2002. Liquefied strength ratio from liquefaction flow failure case histories. *Canadian Geotechnical Journal* **39**, 629–647.

Olson, S.M., Stark, T.D., Walton, W.H., and Castro, G. 2000. 1907 Static liquefaction flow failure of the North Dike of Wachusett Dam. *Journal of Geotechnical and Geoenvironmental Engineering, ASCE* **126**, 1184-1193.

Onate, E., Idelsohn, S.R., Del Pin, F., Aubry, R. 2004. The particle finite element method: an overview, *Int J. Comput Meth*. **1**, 267–307.

Pestana, J.M., Whittle, A.J. 1999. Formulation of a unified constitutive model for clays and sands, *International Journal for Numerical and Analytical Methods in Geomechanics* **23**, 1215–1243.

Pestana, J.M., Whittle, A.J., Salvati, L. 2002. Evaluation of a constitutive model for clays and sands: Part I Sand behavior, *International Journal for Numerical and Analytical Methods in Geomechanics* **26**, 1097–1121.

Poulos, S.J. 1981. The steady state of deformation, *Journal of the Geotechnical Engineering Division, ASCE 107*, 553–562.

Poulos, S.J., Castro, G., France, J. 1985. Liquefaction evaluation procedure, *Journal of the Geotechnical Engineering Division, ASCE* **111**, 772–792.

Pucker., T., Bienen, B., Henke, S. 2013. CPT based prediction of foundation penetration in siliceous sand, *Appl Ocean Res*. **41**, 9–18.

Reid, D. 2015. Estimating slope of critical state line from cone penetration test – an update. *Canadian Geotechnical Journal* **52**, 46 - 57

Robertson, P.K., 1990. Soil classification using the cone penetration test. *Canadian Geotechnical Journal* **27**, 151-158.

Robertson, P.K. 2009. Interpretation of cone penetration tests a unified approach. *Canadian Geotechnical Journal* **46**, 1337-1355

Robertson, P.K. 2010a. Evaluation of flow liquefaction and liquefied strength using the cone penetration test. *Journal of Geotechnical and Geoenvironmental Engineering, ASCE* **136**, 842-853.

Robertson, P.K. 2010b. Estimating in-situ state parameter and friction angle in sandy soils from the CPT. *2nd International Symposium on Cone Penetration Testing*, Paper No. 2-43. CD-Rom.

Robertson, P.K. 2012. In situ soil testing: from mechanics to interpretation. 5th J.K. Mitchell Lecture. *Geotechnical and Geophysical Site Characterization 4* (Eds. Coutinho, Mayne), 3-24. Taylor & Francis Group, London

Robertson, P.K. 2016. Cone penetration test (CPT)-based soil behaviour type (SBT) classification system - an update. *Canadian Geotechnical Journal* **53**, 1910-1927.

Santamarina J.C., Torres-Cruz, L.A., Bachus, R.C. 2019. Why coal ash and tailings dam disasters occur. Knowledge gaps and management shortcomings contribute to catastrophic dam failures. *Science*, **364**, 526-528.

Schnaid, F., Yu, H. S. 2007. Theoretical interpretation of the seismic cone test in granular soils. *Géotechnique*, **57**, 265–272.

Schofield, A. N., Wroth, C. P. 1968. *Critical state soil mechanics*, McGraw-Hill, London.

Seed, H.B., Lee, K.L., Idriss, I.M., Makdisi, F.I. 1975. The slides in the San Fernado Dams during the earthquake of February 9, 1971. *Journal of the Geotechnical Engineering Division, ASCE* **101**, 651-688.

Shuttle, D.A., Cunning, J. 2007. Liquefaction Potential of Silts from CPTu. *Canadian Geotechnical Journal* **44**, 1-19.

Shuttle, D.A., Jefferies, M.G. 1998. Dimensionless and unbiased CPT interpretation in sand. *International Journalof Numerical and Analytical Methods in Geomechanics* **22**, 351-391.

Shuttle, D.A. 2016. Chapter 8 in *Jefferies, M.G., and Been, K. Soil liquefaction: a critical state approach (2nd edition)*. Taylor and Francis, Boca Raton.

Sladen, J.A., D'Hollander, R.D., Krahn, J. 1985a. The liquefaction of sands, a collapse surface approach, *Canadian Geotechnical Journal* **22**, 564–578.

Sladen, J.A., D'Hollander, R.D., Krahn, J., Mitchell, D.E. 1985b. Back analysis of the Nerlerk berm Liquefaction slides, *Canadian Geotechnical Journal* **22**, 579–588.

Solowski, W. T., Sloan, S. W. 2015. Evaluation of material point method for use in geotechnics. *International Journal for Numerical and Analytical Methods in Geomechanics* **39**, 685-701.

Symes, M.J., Gens, A. Hight, D.W. 1984. Undrained anisotropy and principal stress rotation in saturated sand. *Géotechnique*. **34**, 11-27.

Tarragó, D. 2019. *Hydraulic fills liquefaction. Effect on quay stability*. Ph.D. Thesis. Universitat Politècnica de Catalunya, Barcelona.

Taylor, D.W. 1948. *Fundamentals of Soil Mechanics*. John Wiley, New York.

Terzaghi, K. 1957. *Varieties of submarine slope failure.* Norwegian Geotechnical Institute, Publication no. 25, 1–16.

Vaid, Y. P., Chern, J. C. 1985. Cyclic and monotonic undrained response of saturated sands. *Advances in the Art of Testing Soils under Cyclic Conditions*, 120–147. American Society of Civil Engineers.

Vaid, Y.P., Chung, E.K.F., Kuerbis, R.H. 1990. Stress path and steady state. *Canadian Geotechnical Journal* **27**, 1–7.

van't Hoff J., van der Kolff, A.N. (eds.) 2012. *Hydraulic fill Manual*. CRC Press Balkema, Leiden, the Netherlands.

Viana da Fonseca, A. 2013. Application of in situ testing in tailing dams, empahsis on liquefaction. *Geotechnical and Geophysical Site Characterization 4* (Eds. Coutinho, Mayne), 181-203. Taylor & Francis Group, London.

Wroth, C.P., Bassett, R.H. 1965. A stress–strain relationship for the shearing behaviour of a sand. *Géotechnique* **15**, 32–56

Walker, J., Yu, H.S. 2006. Adaptive finite element analysis of cone penetration in clay, *Acta Geotechnica* **1**, 43–57.

Wang, D., Bienen, B., Nazem, M., Tian, Y., Zheng, J., Pucker, T., Randolph M.F. 2015 Large deformation finite element analyses in geotechnical engineering. *Computers and Geotechnics*, **65**,104–14.

Yamamuro, J. A., Lade, P. L. 1998. Steady-state concepts and static liquefaction of silty sands. *J. Geotechmical Geoenvironmental Engineering ASCE* **124**, 868–877.

Yang,,]. 2002. Non-uniqueness of flow liquefaction line for loose sand. *Géoteclmique* **52**, 757-760

Yoshimine, M., Robertson, P.K., Wride, C.E. (Fear) 1999. Undrained shear strength of clean sands to trigger flow liquefaction, *Canadian Geotechnical Journal* **36,** 891–906

Yu, H.S. 1998. CASM: A unified state parameter model for clay and sand. *International .Journal for Numerical and Analytical Methods in Geomechanics* **22**, 621-653.

Yu, H.S. 2006. *Plasticity and Geotechnics*. Springer Science, New York.

Zhang, X., Sloan, S.W., Oñate, E. 2018. Dynamic modelling of retrogressive landslides with emphasis on the role of clay sensitivity, *International Journal for Numerical and Analytical Methods in Geomechanics* **42**, 1806-1822.

Zhou, H., Randolph, M.F. 2009. Numerical investigation into cycling of full-flow penetrometers in soft clay, *Géotechnique,* **59**, 801–12.